Biochemical and pharmacological evaluation of 4-hydroxychromen-2-ones bearing polar C-3 substituents as anticoagulants

ARTICLE *in* EUROPEAN JOURNAL OF MEDICINAL CHEMISTRY · MAY 2012

Impact Factor: 3.45 · DOI: 10.1016/j.ejmech.2012.04.036 · Source: PubMed

European Journal of Medicinal Chemistry 54 (2012) 144–158

Contents lists available at SciVerse ScienceDirect

European Journal of Medicinal Chemistry

journal homepage: http://www.elsevier.com/locate/ejmech

Original article

Biochemical and pharmacological evaluation of 4-hydroxychromen-2-ones bearing polar C-3 substituents as anticoagulants

Milan Mladenović [a,*], Mirjana Mihailović [b], Desanka Bogojević [b], Nenad Vuković [a], Slobodan Sukdolak [a], Sanja Matić [c], Neda Nićiforović [a], Vladimir Mihailović [a], Pavle Mašković [d], Miroslav M. Vrvić [e], Slavica Solujić [a]

[a] Department of Chemistry, Faculty of Science, University of Kragujevac, Radoja Domanovica 12, 34000 Kragujevac, P.O. Box 60, Serbia
[b] Department of Molecular Biology, Institute for Biological Research, University of Belgrade, Bulevar Despota Stefana 142, 11000 Belgrade, Serbia
[c] Department of Biology and Ecology, Faculty of Science, University of Kragujevac, Radoja Domanovica 12, 34000 Kragujevac, P.O. Box 60, Serbia
[d] Faculty of Agronomy, University of Kragujevac, Cara Dušana 34, 32000 Čačak, Serbia
[e] Faculty of Chemistry, University of Belgrade, Studentski Trg 12-16, P.O. Box 158, 11001 Belgrade, Serbia

HIGHLIGHTS

- Fifteen synthesized coumarin compounds were examined as *in vivo* anticoagulants.
- Four compounds, **2b**, **4c**, **5c** and **9c**, presented *in vivo* activity.
- Coumarin molecular target, VKORC1, was homology-modeled.
- Results were discussed using 3D-QSAR, molecular docking and DFT mechanistic studies.
- Coumarin metabolic pathways were obtained.

GRAPHICAL ABSTRACT

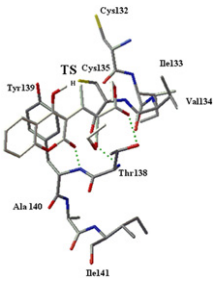

ARTICLE INFO

Article history:
Received 19 April 2011
Received in revised form
10 April 2012
Accepted 25 April 2012
Available online 4 May 2012

Keywords:
4-Hydroxycoumarins
In vivo anticoagulant activity
Metabolic pathways
Homology modeling
Mechanistic studies
3D-QSAR

ABSTRACT

The objective of this study was to investigate *in vitro* and *in vivo* anticoagulant activity of sixteen 4-hydroxycoumarin derivatives bearing polar C-3 scaffolds. The activity was evaluated by measuring prothrombin time. Enhanced anticoagulant activity *in vitro* was observed for all tested compounds. Upon successive administration of 0.5 mg/kg of body weight to adult Wistar rats, over a period of five days, four derivatives (**2b**, **4c**, **5c** and **9c**) presented anticoagulant activity *in vivo*. The most active compound was **2b**, with PT = 30.0 s. Low or non-toxic effects *in vivo* were determined based on the catalytic activity of liver enzymes and the concentration of bilirubin, iron and proteins. Metabolic pathways of the most active compounds *in vivo* were determined after GC/MS analysis of collected rat urine samples. The excretion occurs by glucuronidation of 7-hydroxy forms of tested derivatives. *In vivo* results were described using PLS-based CoMFA and CoMSIA 3D-QSAR studies, which showed CoMFA-SE (q^2 = 0.738) and CoMSIA-SEA (q^2 = 0.763) to be the statistically most relevant models. Furthermore, molecular docking and DFT mechanistic studies performed on the rat VKORC1 homology model revealed interactions between the 4-OH coumarin group in the form of phenolic anion and the Cys135 catalytic site in the transition state.

1. Introduction

Anticoagulant activity of 4-hydroxycoumarins, confirmed by clinical usage of the drug warfarin and expressed through long-term treatment and elongation of International Normalized Ratio,

* Corresponding author. Tel.: +381 34336223; fax: +381 34335040.
E-mail address: mmladenovic@kg.ac.rs (M. Mladenović).

0223-5234/$ – see front matter © 2012 Elsevier Masson SAS. All rights reserved.
doi:10.1016/j.ejmech.2012.04.036

INR [1], prevents many diseases such as venous thrombosis, pulmonary embolism or conditions like heart attack [2]. As an anticoagulant, warfarin acts as a competitive inhibitor of vitamin K-2,3-epoxide reductase subunit 1 (VKORC1), transmembrane protein of liver endoplasmic reticulum [3]. Warfarin prevents reformation of vitamin K-2,3-epoxide to vitamin K and, consequently, vitamin K-dependent synthesis of biologically active forms of clotting factors II, VII, IX and X [1]. The drug is transferred by serum albumin to the active site of VKORC1 in open side chain coumarin form [4]. Since there are still no available PDB, NMR, or X-ray crystallography data structure of warfarin-VKORC1 complex, the active form of warfarin, present during the anticoagulant activity, is debatable. The hemiketal structure of the drug, which is dominant in the crystalline form but minor in solution [5], is not favorable for forming neither the warfarin-albumin nor the warfarin-VKORC1 complex [6]. It has been proposed that warfarin interacts with VKORC1 in deprotonated open side chain coumarin form, *i.e.* the form of phenolic anion [6]. In this form, warfarin shares structural similarities with vitamin K-2,3-epoxide and acts as a competitive inhibitor. Two processes are involved in the anticoagulant activity of warfarin. The first is binding of the 4-phenylpentan-2-one structural part at warfarin C-3 position to Thr138, Tyr139, and Ala140 residues of the VKORC1 active site [7]. The second is interaction between the warfarin 4-hydroxy group, in the form of phenolic anion, and the catalytic center Cys132-Cys135, after which a disulfide bond is formed [3]. Recently, DFT computational studies [8] established a (pseudo-enzymatic) mechanism of vitamin K-2,3-epoxide interaction with VKORC1, on the basis of which the essential epoxide reductase activity can be modeled. The results suggest that the phenolic anion form of warfarin probably acts as a competitive inhibitor of the enzyme [5,6] and that the reaction occurs on the enzyme itself. No actual computational studies on the warfarin inhibition mechanism have been presented so far.

Recently, novel warfarin derivatives in which the phenylpentan-2-one functional group at position C-3 was substituted with various isoprenyl side chains similar to ferulenol, were evaluated as *in vitro* anticoagulants [9]. Study showed that other functional groups, structurally different in comparison with the 4-phenylpentan-2-one, can also contribute the anticoagulant activity [9]. Therefore, this paper presents the *in vitro* and *in vivo* anticoagulant potential of some 4-hydroxycoumarin derivatives that bear polar C-3 substituents and are structurally different from warfarin [10,11]. The C-3 position tested compounds was substituted by various prop-1-en-carbonyl/carboxyl or thiazole-*N*-phenyl functional groups. Their anticoagulant activity was measured by prothrombin time and the INR. The presence of highly hydrophilic C-3 residues contributed to high anticoagulant potential *in vitro* of all compounds. Four of the compounds presented anticoagulant potential *in vivo* after administration of the compounds to adult Wistar rats. The non-toxic behavior of the administered compounds was determined afterwards rat serum screening, using the appropriate biochemical analyses. Monitoring of *in vivo* activity was accompanied by 3D-QSAR studies. The resulting CoMFA and CoMSIA models were used to predict the anticoagulant activity of sixteen novel designed compounds. In order to describe the *in vivo* results trough the interactions of our derivatives with VKORC1, we built a homology model of rat VKORC1 and performed molecular docking studies. Since no results of similar studies have been presented before, we proposed a pseudo-enzymatic mechanism of antagonist behavior of our derivatives and studied it computationally with the aid of DFT theory.

2. Chemistry

In our previous papers, synthesis and structural characterization of 16 substituted chromene-*2H*-one derivatives (**1**–**10c**) were reported (Scheme 1) [10,11]. The compounds were characterized by elemental analysis (C, H, N, O, and S). Structural characterization was carried out by IR, H^1 NMR and MS analyses. Over 95% of chemical purity of the synthesized compounds was confirmed with HPLC and MS.

3. Results and discussion

3.1. In vitro anticoagulant activity

The coagulation and prothrombin times of human plasma were normal: CT = 105 and PT = 11.0–14.5 s (Table 1), respectively. In comparison with the activity of warfarin (measured PT = 18.5 s), the introduction of prop-1-en-carbonyl/carboxyl (**2**–**8b**) and thiazole-*N*-phenyl scaffolds (**2**–**10c**) at the coumarin C-3 position greatly increased the anticoagulant activity.

The C-3 position of the 4-xydroxycoumarin core within **2**–**8b** was substituted with *trans*-oriented carboxyl or ester groups and various *cis*-oriented groups with respect to the methyl group of the prop-1-en scaffold. Among **2**–**8b**, the highest prolongation of prothrombin time was noticed after testing **2b**, a *cis*/*trans*-

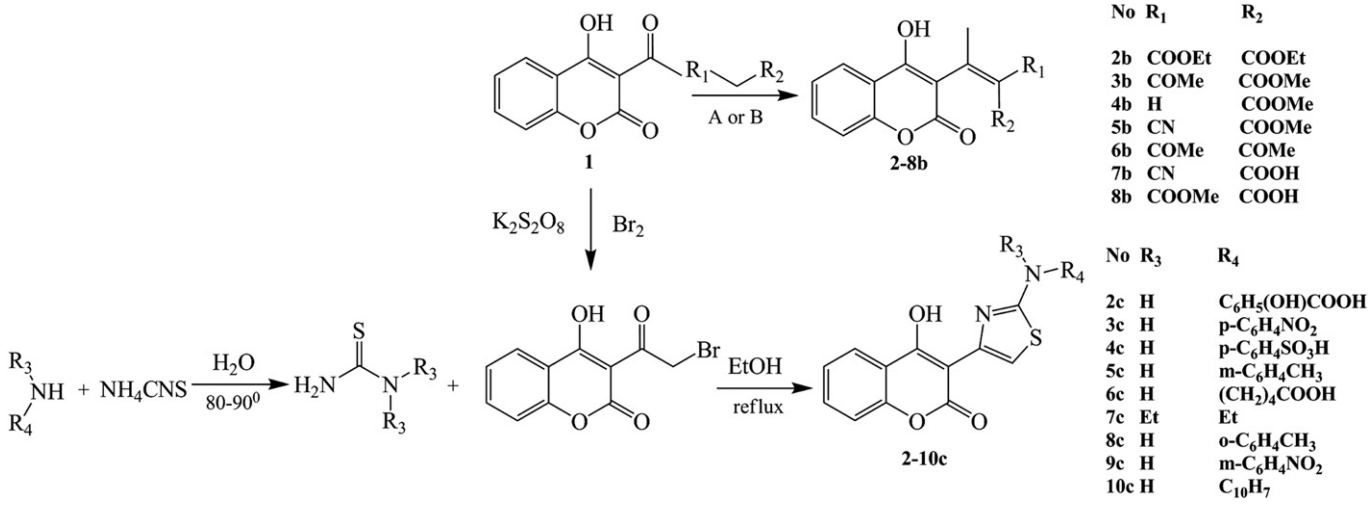

No	R_1	R_2
2b	COOEt	COOEt
3b	COMe	COOMe
4b	H	COOMe
5b	CN	COOMe
6b	COMe	COMe
7b	CN	COOH
8b	COOMe	COOH

No	R_3	R_4
2c	H	$C_6H_5(OH)COOH$
3c	H	p-$C_6H_4NO_2$
4c	H	p-$C_6H_4SO_3H$
5c	H	m-$C_6H_4CH_3$
6c	H	$(CH_2)_4COOH$
7c	Et	Et
8c	H	o-$C_6H_4CH_3$
9c	H	m-$C_6H_4NO_2$
10c	H	$C_{10}H_7$

Scheme 1. Synthesized 4-hydroxy-chromene-2-one derivatives.

Table 1
Anticoagulant activity of coumarin derivatives *in vitro* and *in vivo* (after 24 h and five-day treatment).

Comp.	PT *in vitro*[a]	INR[b]	PT *in vivo*[c]	INR	PT *in vivo*[d]	INR	Fibrinogen. (g/L)	FT *in vivo*[e]
1	14.0 ± 0.2[f]	1.25	9.1 ± 0.2	0.9	9.5 ± 0.2	0.9	2.5 ± 0.2	44.9 ± 0.7
2b	23.0 ± 0.1	1.99	10.3 ± 0.3	0.13	10.5 ± 0.1*,†	0.13	5.1 ± 0.1	51.3 ± 0.5
					30.0 ± 0.2[g,*]	0.13	1.6 ± 0.1	
3b	19.0 ± 0.2	1.80	9.3 ± 0.1	0.92	9.8 ± 0.2	0.94	1.6 ± 0.2	40.7 ± 0.4
4b	20.0 ± 0.3	1.90	8.0 ± 0.2	0.64	9.0 ± 0.3	0.67	1.8 ± 0.4	35.2 ± 0.3
6b	17.0 ± 0.2	1.55	8.6 ± 0.2	0.69	9.6 ± 0.2	0.72	2.47 ± 0.2	24.6 ± 0.4
7b	21.0 ± 0.1	2.25	8.2 ± 0.2	0.66	9.2 ± 0.1	0.69	0.5 ± 0.1	196.8 ± 0.6
8b	20.0 ± 0.1	1.90	5.7 ± 0.4	0.37	8.7 ± 0.1	0.48	3.2 ± 0.5	19.4 ± 0.5
2c	22.0 ± 0.3	2.15	8.8 ± 0.2	0.67	9.1 ± 0.3	0.86	4.2 ± 0.2	55.7 ± 0.5
3c	25.0 ± 0.4	2.44	8.1 ± 0.1	0.65	9.1 ± 0.4	0.68	1.8 ± 0.3	33.7 ± 0.4
4c	26.5 ± 0.2	2.60	10.4 ± 0.1	0.82	12.4 ± 0.2*,†	0.84	/	>500
					28.6 ± 0.1[g,*]	1.38	0.9 ± 0.1	
5c	25.0 ± 0.2	2.44	9.6 ± 0.2†	1.16	9.7 ± 0.2†	1.16	2.0 ± 0.1	27.6 ± 0.6
					28.1 ± 0.2[g,*]	1.34	1.2 ± 0.1	
6c	22.0 ± 0.3	2.10	8.0 ± 0.2	0.64	10.0 ± 0.3	0.67	2.5 ± 0.2	23.9 ± 0.4
7c	18.5 ± 0.1	1.75	8.0 ± 0.3	0.64	10.0 ± 0.1	0.67	1.4 ± 0.3	44.9 ± 0.5
8c	18.1 ± 0.2	1.70	8.1 ± 0.4	0.68	8.1 ± 0.2	0.68	2.1 ± 0.2	28.7 ± 0.4
9c	24.4 ± 0.6	2.30	9.6 ± 0.2†	0.94	14.4 ± 0.6*,†	1.14	0.6 ± 0.2	>500
					28.1 ± 0.1[g,*]	1.34	1.74 ± 0.2	
10c	27.5 ± 0.1	2.70	9.2 ± 0.2	0.94	9.7 ± 0.1	0.94	1.9 ± 0.2	33.2 ± 0.4
C	13.2 ± 0.1	1.15	9.2 ± 0.4	0.91	9.7 ± 0.2	0.91	1.8 ± 0.3	111.9 ± 0.3
					12.1 ± 0.2[g]	0.86	1.9 ± 0.3	
W[h]	18.5 ± 0.1	1.73	10.3 ± 0.2	0.83	12.2 ± 0.4	0.83	1.9 ± 0.3	33.4 ± 0.5
					LD[i]			

*p <0.05 when compared with the negative control; † <0.05 when compared with the positive control.
[a] Prothrombin time measured on the human plasma measured in sec.
[b] International Normalized ratio.
[c] The prothrombin time measured after 0.1 mg/kg coumarin administration measured in sec.
[d] The prothrombin time measured after 0.5 mg/kg coumarin administration measured in sec.
[e] Fibrin time measured in sec.
[f] Results are given with standard deviation, calculated from at least three measurements.
[g] The prothrombin time measured after the second 0.5 mg/kg administration of coumarin derivatives.
[h] Warfarin.
[i] Lethal dose.

carboxyethyl derivative (PT = 23.0 s). A minor decrease in activity was detected for **7b**, *cis*-cyano and *trans*-carboxyl derivative, with a prothrombin time of 21.0 s. A level of activity comparable to **7b** was recorded for **8b**. In the structure of **8b**, besides the presence of the *trans*-carboxyl group, there is a *cis*-carboxymethyl residue, which additionally contributes to the activity. Further decrease in the anticoagulant potential was observed for **4b** and **3b**. The lower potential of these compounds is related with the absence of carboxyl or cyano groups in the *cis*-position.

The substitution of prop-1-en moieties with various thiazole-*N*-phenyl groups (**2**–**10c**) further enhanced the anticoagulant potential in the following order: **9c** < **3c**, **5c** < **4c** < **10c**. Thus, by changing the nitro group position from *m*- (**9c**) to *p*- (**3c**), the prothrombin time was increased. The **5c** (*m*-CH_3) and **3c** derivatives presented equal activity (PT = 25.0 s). The *p*-sulfo (**4c**) and *N*-naphthyl (**10c**, PT = 27.5 s) compounds attained the highest activity *in vitro.*

3.2. In vivo anticoagulant activity

3.2.1. Observed activity

A short period of intraperitoneal (*i.p.*) administration of compounds **1**–**10c** to adult Wistar rats in a concentration of 0.1 mg/kg of body weight did not produce the noteworthy increase of anticoagulant activity in comparison to warfarin (Table 1). There was no significant statistical difference between the activity of warfarin, **2b**, and **4c**, while the activity of **5c** and **9c** was 6.89% lower comparing with the clinical drug.

Increase of the dose (0.5 mg/kg of body weight) resulted in a better activity (Table 1) and showed four compounds, prop-1-en diethylmalonate derivative **2b** (PT = 10.5 s), *N*-thiazole *p*-sulfonic acid derivative **4c** (PT = 10.4 s), *N*-thiazole *m*-methyl derivative **5c** (PT = 9.7 s) and *N*-thiazole *m*-nitro derivative **9c** (PT = 14.4 s) to be comparable with warfarin and potential *in vivo* anticoagulants. With respect to the prothrombin time of the negative control (*i.e.* plasma containing no anticoagulants), the activities of **2b**, **4c,** and **9c** were 1.08-, 1.27- and 1.48-fold above the control value, respectively. There was no significant statistical difference between the prothrombin time measured in plasma containing **5c** and the negative control. The activities of **4c** and **9c** were 1.18-fold above, while the activities of **2b** and **5c** were 86.06 and 79.51% of the activity of warfarin as the positive control.

In view of the known behavior of warfarin to exert anticoagulant activity after long-term administration, the test animals were subjected to repeated five-day treatment with the selected compounds in a concentration of 0.5 mg/kg of body weight. Such treatment significantly increased the prothrombin time (Table 1). Since continuous *i.p.* administration of warfarin induced death of the treated animals on the final day, measurement of prothrombin time was not possible. Statistical comparisons were therefore taken only for the administered compounds and negative control. An excellent *in vitro-in vivo* activity correlation was observed for **2b** on the rat model with prothrombin time *in vivo* of PT = 30.0 s, *i.e.* 2.5-fold above the basic value measured in the negative control. The range of activities of **4c**, **5c**, and **9c** was 28.1–28.6 s, 2.3- to 2.34-fold above the negative control values.

3.2.2. Liver status after in vivo administration of coumarin derivatives

The toxicity level of the derivatives used in this study was evaluated by measuring the catalytic activities of ALT, AST, ALP, and γ-GT in serum as hepatocellular markers, and by monitoring bilirubin concentration as a hepatobiliary marker (Table 2) [12–14]. In both cases, measurements were performed after *i.p.* administrations (0.5 mg/kg). The ALT and AST catalytic activities

are sensitive indicators of acute liver damage [12]. Bilirubin concentration is a useful clinical clue for the diagnosis of hepatocyte necrosis [15]. The amounts of Fe and serum proteins were observed as well.

In general, after the first animal treatment with coumarin derivatives in concentration of 0.5 mg/kg of body weight, most of the compounds were weak inflammation agents, as judged from low increase in the catalytic activity of serum AST and the concentration of ferrous ions [16,17]. In serum containing **2b**, **4c**, **5c**, and **9c**, catalytic activity of AST was significantly increased: 1.41-, 1.59-, 1.68-, and 1.74-fold above the activity in negative control, respectively. Still, the administration of **2b**, **4c**, and **5c** induced lower catalytic activity of the enzyme than in the serum of animals treated with warfarin (63.28–97.26% of the basal level), and therefore lower inflammation than induced by the clinical drug. The compound **9c** was the strongest inflammation agents, with toxicity expressed by AST catalytic activity value 1.06-fold above the positive control.

During continued 0.5 mg/kg administration, no inflammation was perceived after treatment of rats with the compounds. The catalytic activities of AST measured in serum containing **2b**, **4c**, **5c**, and **9c** were respectively 6.25, 7.33, 21.62, and 5.90% lower than in the negative control.

The low catalytic activities of ALT and ALP recorded after the first and second 0.5 mg/kg administration indicated that there was no chemically induced liver damage [18], which was also confirmed by no change in the concentration of serum proteins [18]. Further, the decrease of bilirubin concentration and normal catalytic activity of γ-GT showed that our derivatives do not affect the bile [18].

The *in vivo* anticoagulant potential of tested 4-hydroxycoumarins was attained after five-day long administration of a 0.5 mg/kg concentration. The results are in correlation with the fact that coumarin presents anticoagulant activity after several days of continuous treatment. Furthermore, analyses of the rat liver by biochemical serum screening showed that coumarin-conditioned inflammation decreased after the administration interval, and no inflammation was observed on the final day of application.

3.2.3. Determination of coumarin metabolites from rat urine by GC/MS

The dominant pathway in the first phase of coumarin metabolism in rats and mice is hydroxylation of the coumarin core at the C-7 position, catalyzed by the CYP2A5 enzyme, which belongs to the CYP450 family [19]. Our GC/MS analysis was therefore directed towards the detection of 7-hydroxy forms of the administered compounds. The molecular ions of the tested compounds recorded in ethanol solution were M^+-1 m/z 345, 415, 349 and 380 for **2b**, **4c**, **5c**, and **9c**, respectively. Hence, after the first phase of metabolism, the expected M^+ m/z values for 7-hydroxy forms were 362, 432, 366, and 397. The detection of particular ions in the mass spectra of hydrolyzed urine samples suggested that the tested derivatives were metabolized in the same way as the coumarin core (Scheme 2). The presence of 7-hydroxycoumarin forms of **2b**, **4c**, **5c**, and **9c** was confirmed by correlation of the obtained spectra with the spectrum of umbelliferone. The mass of m/z 165 for 7-hydroxycoumarin which was detected in the spectra of hydrolyzed urine samples containing **2b**, **4c**, **5c**, and **9c** differs from the recorded mass of umbelliferone (M^+ m/z 162) [20] due to the transfer of hydrogen atoms towards the coumarin core during fragmentation of **2b**, **4c**, **5c**, and **9c**. On the other hand, the similar intensities of the compared ions, viz., m/z 165 and m/z 162, indicated that they belong to the same molecular species. Further confirmation that m/z 165 originates from the coumarin core was the presence of m/z 146 or 147 ions, which correspond to M^+ of the coumarin molecule [18]. Hydroxylation may also occur in positions C-5, -6, and -8 [5], but these transformations are not favorable for coumarin excretion. The second phase of coumarin metabolism is mainly catalyzed by UDP-glucuronyltransferase resulting in formation of the coumarin-7-glucuronide form, in which the molecule is excreted [19]. Hence, it is presumed that excretion of the tested derivatives occurs after the formation of **2b**-, **4c**-, **5c**-, and **9c**-glucuronides. A much smaller amount of excretion occurs after the formation of coumarin-7-sulfate, catalyzed by sulfotransferase [19]. There was no evidence for the formation of other metabolites using the specified GC/MS conditions.

Table 2
Hepatotoxic activity of coumarin derivatives and liver protein status after 24 h and five-day treatment in concentration of 0.5 mg/kg of body weight.

Comp.	Bilirubin(μmol/L)	AST (U/L)	ALT (U/L)	ALP (U/L)	γ-GT (U/L)	Fe (μmol/L)	Proteins (g/L)	Albumin (g/L)
1	1.7 ± 0.1	160.5 ± 0.4	34.8 ± 0.2	200 ± 0.4	3.8 ± 0.1	26.1 ± 0.1	63.8 ± 0.6	31.9 ± 0.6
2b	2.0 ± 0.2	238.3 ± 0.2*,†	71.8 ± 0.3	513 ± 0.7	3.1 ± 0.2	28.4 ± 0.3	67.2 ± 0.5	35.2 ± 0.5
		209.9 ± 0.2[a,*]	55.5 ± 0.3[b]		2.3 ± 0.2[c]	17.7 ± 0.3[d]		
3b	1.7 ± 0.3	236.9 ± 0.3	65.5 ± 0.2	285 ± 0.3	2.8 ± 0.1	23.9 ± 0.4	66.4 ± 0.3	38.9 ± 0.4
4b	1.4 ± 0.2	154.3 ± 0.2	57.2 ± 0.2	333 ± 0.9	3.0 ± 0.3	54.2 ± 0.5	65.2 ± 0.4	39.0 ± 0.1
6b	1.5 ± 0.4	201.4 ± 0.4	56.4 ± 0.4	223 ± 0.5	4.4 ± 0.1	32.4 ± 0.3	66.5 ± 0.2	40.6 ± 0.6
7b	/	/	/	/	/	/	68.9 ± 0.6	38.6 ± 0.3
8b	1.8 ± 0.2	218.4 ± 0.3	51.8 ± 0.6	215 ± 0.6	4.4 ± 0.1	19.4 ± 0.2	62.8 ± 0.3	35.8 ± 0.5
2c	1.9 ± 0.2	232.5 ± 0.2	44.3 ± 0.3	213 ± 0.4	3.6 ± 0.2	22.6 ± 0.4	65.8 ± 0.4	37.4 ± 0.3
3c	1.7 ± 0.5	264.4 ± 0.2	68.7 ± 0.4	204 ± 0.8	3.8 ± 0.3	14.8 ± 0.3	63.0 ± 0.4	37.2 ± 0.4
4c	1.6 ± 0.1	269.7 ± 0.2*,†	58.4 ± 0.3	164 ± 0.6	2.4 ± 0.2	19.3 ± 0.2	64.9 ± 0.2	40.8 ± 0.4
		207.5 ± 0.2[a,*]	63.0 ± 0.3[b]		2.2 ± 0.2[c]	19 ± 0.2d		
5c	1.8 ± 0.2	284.6 ± 0.2*,†	67.3 ± 0.3	172 ± 0.2	2.2 ± 0.2	28.4 ± 0.4	66.2 ± 0.7	41.9 ± 0.1
		175.5 ± 0.2[a,*]	62.4 ± 0.3[b]		3.0 ± 0.2[c]	17.3 ± 0.4[d]		
6c	1.2 ± 0.1	231.5 ± 0.2	52.6 ± 0.2	246 ± 0.4	3.5 ± 0.2	27.4 ± 0.6	71.5 ± 0.1	35.4 ± 0.2
7c	2.0 ± 0.3	254.8 ± 0.1	64.7 ± 0.1	192 ± 0.7	4.4 ± 0.2	25.0 ± 0.2	63.2 ± 0.6	36.7 ± 0.5
8c	1.8 ± 0.1	263.4 ± 0.2	59.5 ± 0.3	318 ± 0.4	3.6 ± 0.1	29.2 ± 0.4	69.2 ± 0.3	36.3 ± 0.1
9c	2.2 ± 0.2	294.6 ± 0.3*,†	52.4 ± 0.1	225 ± 0.4	2.8 ± 0.2	29.7 ± 0.1	64.2 ± 0.4	39.7 ± 0.2
		210.7 ± 0.3[a,*]	65.1 ± 0.1[b]		2.6 ± 0.2[c]	17.3 ± 0.1[d]		
10c	2.0 ± 0.2	345.3 ± 0.2	85.0 ± 0.2	210 ± 0.3	4.3 ± 0.1	24.6 ± 0.2	72.8 ± 0.2	41.3 ± 0.2
C	2.4 ± 0.5	169.0 ± 0.2	76.8 ± 0.4	516 ± 0.2	4.0 ± 0.2	44.2 ± 0.2	71.8 ± 0.5	39.3 ± 0.4
		223.9 ± 0.2[a]	40.7 ± 0.4[b]		4.5 ± 0.2[c]	21.1 ± 0.2[d]		
W	1.3 ± 0.2	277.3 ± 0.1	51.5 ± 0.4	170 ± 0.6	3.4 ± 0.1	22.3 ± 0.4	59.4 ± 0.4	34.5 ± 0.2

*p <0.05 when compared with the negative control; † <0.05 when compared with the positive control.
[a] The level of AST after the second 0.5 mg/kg coumarin administration.
[b] The level of ALT after the second coumarin administration.
[c] The level of γ-GT ather the second coumarin administration.
[d] The level of Fe after the second coumarin administration.

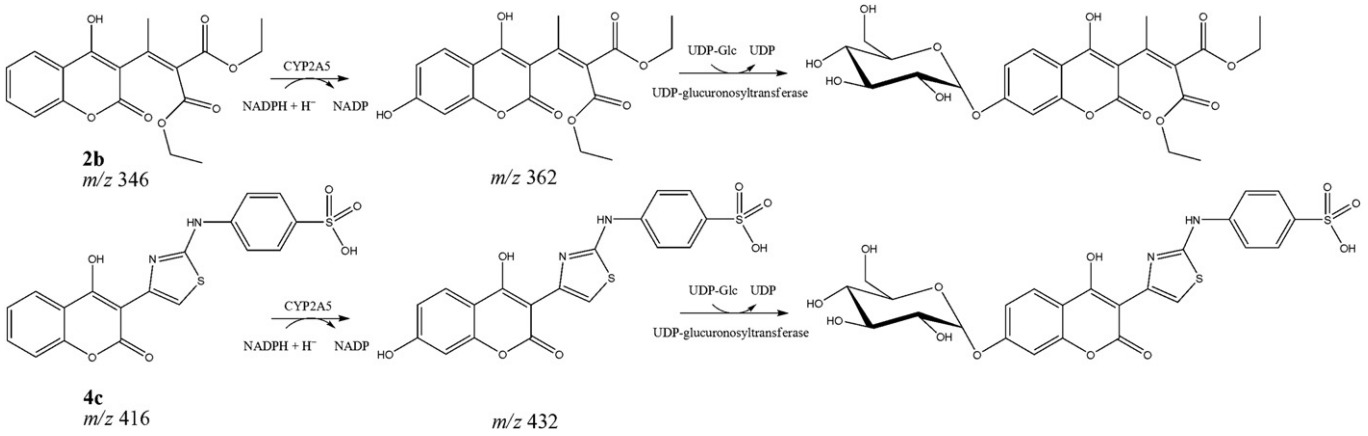

Scheme 2. Proposed metabolic pathways of **2b** and **4c**.

3.2.4. CoMFA and CoMSIA results

As a result of the 3D-QSAR studies, CoMFA and CoMSIA contour maps were generated to rationalize the pharmacologically active regions in 3D space around the molecules. The positions of steric, electrostatic, and hydrogen bond fields were used to define parts of molecules that enhance or lessen activity. Contour maps were generated to reveal the nature of potential interactions between the 4-OH group of coumarin anticoagulants and the catalytic site, as well as between the C-3 polar scaffolds and amino acids of the active site of the VKORC1 molecule.

Fig. 1. depicts aligned molecules within the grid box (grid spacing of 2.0 Å) used to generate the CoMFA and CoMSIA columns.

The best obtained CoMFA model described the anticoagulant activity of the evaluated compounds using both steric and electrostatic fields (CoMFA-SE), had a cross-validated coefficient value of $q^2 = 0.738$ with an optimized component number of $N = 6$, excellent non-validated value of $r^2 = 0.931$, and standard estimate error (SEE) of 0.224. The model possessed a low standard deviation ($s = 0.216$) and a high Fisher ratio ($F = 108.96$). Statistical parameters of the model suggested that it should be a useful tool for the prediction of IC_{50} values, *i.e.* the concentrations that increase the prothrombin time for 50%. Within the CoMFA-SE model, similar contributions of both steric and electrostatic fields (49.1 and 51.9%, respectively) were noticed. Correlations between the calculated and experimental pIC_{50} values (from training and LOO cross-validation) are illustrated in Fig. 2(a). The CoMFA-SE model was also used to predict anticoagulant activity of the test-set compounds. This model was able to describe the test-set variance with $r^2 = 0.724$ and a standard deviation of test-set predictions of (s_{test}) = 0.901. The predicted values of test-set are listed in Table 3. Our analysis revealed that the proposed model was able to successfully predict the activity of compounds that were not used in the training process.

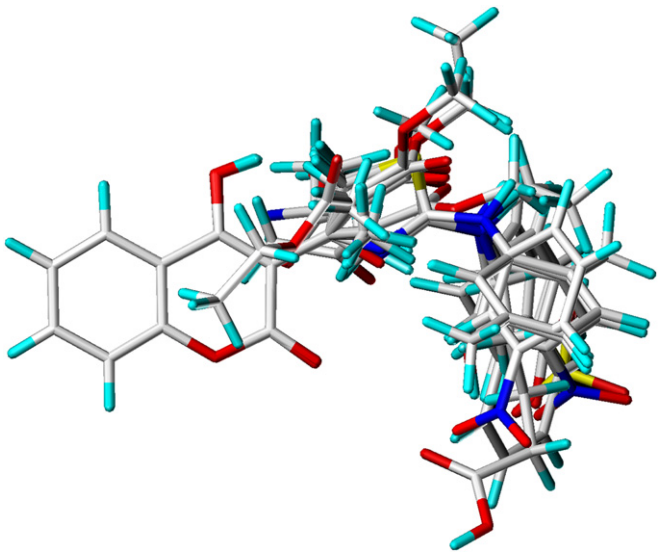

Fig. 1. Atom-by-atom superposition used for the 3D-QSAR analysis.

The positions of contour plots of CoMFA steric and electrostatic fields surrounding the **2b** and **4c**, as the most promising anticoagulants *in vivo*, are presented in Fig. 3.

The steric fields are characterized by green and yellow isopleths, which represent steric regions that favor and disfavor activity, respectively. Green isopleths (Fig. 3(a) and (b)) are placed above both carbonyl groups of the C-3 diethylmalonate scaffold of **2b** as well as the thiazole-*N*-Ph-SO_3H system of **4c**. The *m*-CH_3 and *m*-NO_2 groups of **5c** and **9c**, respectively, are also overlaid with green contours. These contours indicate residues that are mandatory for a high anticoagulant activity and expected to bind with the VKORC1 active site. Yellow isopleths cover the space around the methyl group of the prop-1-en moiety, ethyl group of the *trans*-carboxyethyl residue of **2b**, and the sulfur atom of the thiazole ring of **4c**. This suggests that regions covered with the yellow contours are too large, *i.e.* not favorable for activity. Similar orientation of unfavorable fields was observed above the structures of **5c** and **9c**.

The electrostatic fields are depicted in Fig. 3(c) and (d). The blue contours illustrate electrostatic regions where an increase of positive charge and electron-donor ability of functional groups enhance activity, while red isopleths indicate regions where negative charge and electron-withdrawing groups are favorable for activity. The blue electrostatic maps around the hydrogen atom of the 4-OH group of both **2b** and **4c**, as well as of **5c** and **9c**, show that positively charged hydrogen atom is very important for the overall activity and that it participates in the anticoagulant mechanism. Furthermore, the blue regions that cover *cis*-carboxyethyl group of **2b** and phenyl group of **4c** suggest that the presence of the electron-donating groups increase the activity. Location of the red contour surrounding the *cis*-carboxyethyl group of **2b** shows the significance of groups containing electron-withdrawing oxygen atoms for the activity. Also, apart from the unfavorable steric effects of thiazole sulfur, the low positive charge of the sulfur atom is important for the activity of **4c**. Electrostatic interactions established over the sulfur atom are important for the activity of **5c** and **9c**, as well.

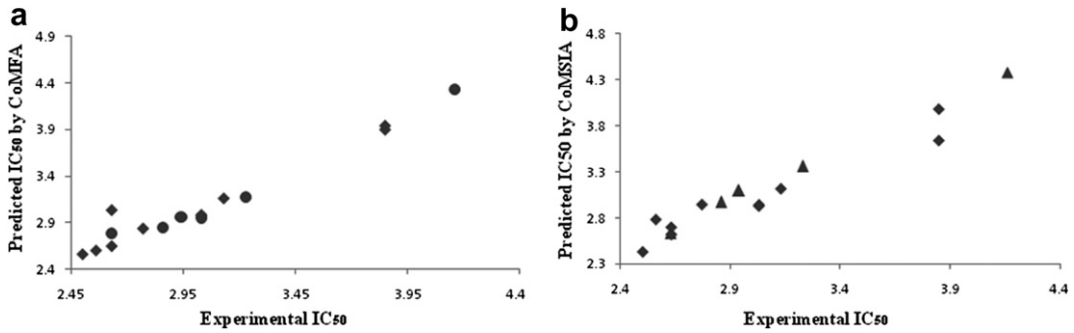

Fig. 2. a) Plot of predicted *vs.* experimental pIC_{50} values of the training set (squares) and the test-set (circles) by CoMFA; b) Plot of predicted versus experimental pIC_{50} values of the training set (squares) and the test-set (triangles) by CoMSIA.

In comparison with CoMFA methodology, CoMSIA has the advantage of exploring more fields. A statistically more significant model was obtained using the CoMSIA study. The best CoMSIA model (CoMSIA-SEA) included steric, electrostatic, and H-bond acceptor (HA) fields and had a q^2 value of 0.763 with optimized components of $N = 3$, a non-cross-validated correlation coefficient value r^2 of 0.916, and an SEE value of 0.224. The model possessed a low standard deviation ($s = 0.791$) and a high Fischer ratio ($F = 78.96$). Statistical parameters of the model suggested that it should be a useful tool for the prediction of IC_{50} values. Contributions of the steric, electrostatic, and HB acceptor fields within the CoMSIA-SEA model were 11.2, 42.6, and 46.2%, respectively. The predictions of pIC_{50} values of the training set are shown in Table 3. Correlations between the calculated and experimental pIC_{50} values (from training and LOO cross-validation) are shown in Fig. 3(b). The CoMSIA-SEA model was also used to predict inhibitory activities of the test-set compounds. It was found that this model was able to describe the test-set variance with $r^2 = 0.817$ and $s_{test} = 0.766$.

The contour plots of the CoMSIA steric, electrostatic, and HB acceptor fields are presented in Fig. 4. To simplify, only interactions between the most active compounds and the contour maps are shown.

Green isopleths around **2b** and **4c**, depicted by Fig. 4(a) and (d) respectively, illustrate regions where bulky groups favor the activity, while yellow isopleths present regions that decrease it. Thus, carbonyl groups in the C-3 residue of **2b** are surrounded by the advantageous side of the steric field, indicating their importance in interactions with the molecular target. In the case of **4c**, green contours encircle nitrogen atoms of the thiazole and amino group, respectively. A similar position of the fields was perceived for **5c** and **9c**. The CoMSIA steric field contour maps were similar to the corresponding CoMFA contour maps.

Electrostatic fields of **2b** and **4c** are depicted by Fig. 4(b) and (e), respectively. Blue contours depict regions where positive electrostatic interactions increase the activity, while red contours indicate regions where negative electrostatic interactions also increase the activity. Positive electrostatic regions are located above carbonyl group of *cis*-carboxyethyl scaffold of **2b** and the sulfur atom of *p*-SO_3H group of the **4c**. The orientation of a blue contour around the sulfo group was the main difference in comparison with the CoMFA field, where only the phenyl group was surrounded by the contour. Negative electrostatic fields are positioned around the hydrophobic parts of the molecules. As for **5c** and **9c**, blue contours cover the sulfur atom of the thiazole ring, while a strong red contour was noticed around the *p*-nitro group of **9c**, highlighting the electron-withdrawing effect as important for activity.

The contour maps representing hydrogen bond acceptor fields of **2b** and **4c** are depicted in Fig. 4(c) and (f), respectively. The magenta isopleths represent areas where HB acceptor groups increase activity. Large magenta contours cover both carbonyl residues of the **2b** C-3 scaffold and *N*-thiazole system of **4c**. The red regions decrease the ability of the compounds to accept a proton and form a hydrogen bond. They are located around the ethyl group of the *cis*-carboxyethyl scaffold of **2b** and the amino group that links the thiazole and phenyl group of **4c**. The position of the red fields indicates that the presence of ethyl group as well as secondary amine group as a strong H-bond donor are detrimental to biological activity. Indeed, the potential of carboxyl groups as HB acceptors in the structure of **2b** was stronger than the HB acceptor

Table 3
Regression summaries of CoMFA and CoMSIA results and the prediction of the pIC_{50} of newly designed compounds.

Comp.	pIC_{50}	CoMFA		CoMSIA		Designed	CoMFA		CoMSIA	
	Exp.	Pred.	Res.	Pred.	Res.	Comp.	Pred.	Res	Pred.	Res
1	2.77	2.83	0.06	2.95	0.05	**1d**	3.97	0.05	3.92	0.07
2b	3.85	3.94	0.30	3.38	0.37	**2d**	3.95	0.09	3.87	0.44
3b	2.94	2.96	0.28	3.10	0.26	**3d**	4.04	0.35	3.99	0.15
4b	2.56	2.60	0.14	2.58	0.22	**4d**	3.98	0.12	3.81	0.09
6b	2.86	2.84	0.41	2.97	0.40	**5d**	4.14	0.41	4.06	0.25
7b	2.63	2.65	0.02	2.70	0.03	**6d**	4.10	0.08	4.03	0.35
8b	2.50	2.56	0.06	2.43	0.06	**7d**	4.21	0.24	4.12	0.14
2c	2.63	2.79	0.46	2.63	0.27	**8d**	4.14	0.56	4.08	0.04
3c	2.63	3.04	0.40	2.62	0.38	**9d**	4.22	0.58	4.07	0.02
4c	3.85	3.90	0.14	3.84	0.12	**10d**	4.18	0.13	4.11	0.19
5c	4.16	4.33	0.83	4.38	0.63	**11d**	4.13	0.25	3.98	0.41
6c	3.03	2.95	0.08	2.95	0.07	**12d**	3.87	0.34	3.44	0.52
7c	3.03	2.98	0.04	2.93	0.08	**13d**	4.07	0.27	4.06	0.38
8c	2.27	2.25	0.98	2.26	0.42	**14d**	4.09	0.41	4.11	0.72
9c	3.13	3.16	0.04	3.12	0.05	**15d**	4.15	0.03	4.10	0.65
10c	3.23	3.17	0.05	3.36	0.18	**16d**	4.12	0.15	4.07	0.28

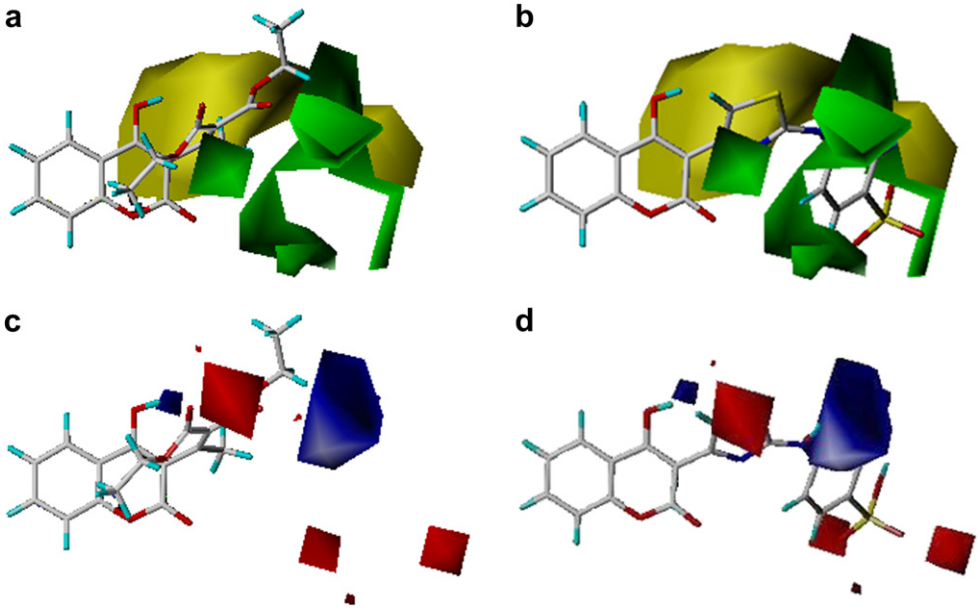

Fig. 3. CoMFA contour a) Steric and c) Electrostatic maps of **2b**; b) Steric and d) Electrostatic maps of **4c**.

ability of the *N*-thiazol groups in the structures of **4c**, **5c**, and **9c**, thereby ensuring better *in vivo* activity of **2b**.

Regression summaries of CoMFA and CoMSIA results and the prediction of the pIC_{50} of newly designed compounds.

3.2.5. Homology modeling and study of the binding mode onto rat VKORC1

The complete three-dimensional structure of rat VKORC1 is not available yet, for either experimental or theoretical reasons. For the purpose of molecular docking studies, we created a homology model of rat VKORC1. The crystallographic structure of *Synechococcus* sp. bacterial vitamin K epoxide reductase was chosen as the template structure for computer simulations. The goal of homology modeling was to achieve four transmembrane α-helix structures (amino acid positions 11–31; 81–97; 101–123; 127–149) [3] (Fig. 5(b)) and the best possible loop alignment (Fig. 5(a)). After successful modeling, the structure of rat VKORC1 was relaxed by molecular dynamics simulation; the calculated Cα root-mean-square deviation (rmsd) value of 0.24 nm at 720 ps confirmed that the protein reached a state of equilibration during MD simulations. On the other hand, the relatively low sequence identity between bacterial and rat VKORC1 in extracellular regions made it difficult to predict exact loop conformations in the specified regions of the homology-modeled protein. Still, high identity (59%) in the 1–161 amino acid sequence between rat and bacterial VKORC1 provided excellent alignment between the modeled and template structure in the transmembrane region of the protein. This was the basis for successful molecular docking of the most active compounds *in vivo* on the selected equilibrium structure.

Docking simulations have further revealed the considerable role of the C-3 residues in anticoagulant activity of evaluated derivatives (Fig. 6).

Thus, the lowest energy conformation of **2b** is stabilized within the active site of rat VKORC1 by the formation of three hydrogen bonds (Fig. 6(a)). The carbonyl group of the lactone part of the 4-hydroxycoumarin core of **2b** is oriented towards the formation of the first, strong hydrogen bond with the NH group of the peptide bond of Tyr139 (d = 1.896 Å). The second hydrogen bond is formed between the carbonyl group of the *cis*-carboxyethyl scaffold and the hydroxyl group of Thr138 (d = 2.626 Å). Finally, the ethoxy group oxygen of the *trans*-carboxyethyl scaffold is positioned within hydrogen-bonding distance (d = 2.115 Å) from the NH group of the peptide bond between the Thr138 and Tyr139. The exact hydrogen-bonding orientation correlates perfectly with the position of CoMFA and CoMSIA steric, CoMSIA electrostatic, and hydrogen bond acceptor contours, which showed carbonyl groups of the **2b** C-3 scaffold to be particularly important for activity. Such compact interaction of **2b** with the enzyme influenced low K*i* value of 68.9 μM. Further, advantageous alignment of the hydrogen atom within 4-OH group of **2b** towards Cys135 (d = 1.720 Å) is assured trough electrostatic interactions between the hydroxyl group of Tyr139 and the 4-OH group. This interaction is predicted by the blue CoMFA electrostatic contour. The obtained active site enzyme-substrate conformation points to Cys135 as an amino acid participating in the coagulation mechanism.

The spatial arrangement of **4c** (Fig. 6 (b)) led to extension of the binding space in VKORC1 to one more amino acid, Ile141. Still, orientation of the coumarin ring itself was quite similar compared to **2b**. Inspection of the **4c** binding mode reveals several positive interactions. Thus, the *p*-sulfo group is narrowed to Ile141, presenting one S=O group as an acceptor for one strong hydrogen bond with the NH group of the peptide bond between Ala140 and Ile141 (d = 1.324 Å). The interaction is predicted by the CoMFA steric and CoMSIA electrostatic isopleths. The coumarin ring is stabilized by two electrostatic interactions. First one is the interaction between the lactone oxygen atom of **4c** and the carbonyl group of the peptide bonds between Thr138 and Tyr139. The second interaction occurs between the carbonyl oxygen atom of the lactone group and amino group of the peptide bond of Tyr139 and Ala140. Orientation of the 4-OH group is stabilized by electrostatic interactions with the Tyr139 hydroxyl group, as in **2b**, placing the hydrogen atom in suitable orientation towards Cys135 (d = 1.735 Å). The obtained CoMFA electrostatic contours predicted this interaction. Further, positive hydrophobic interaction between the phenyl residues of **4c** and Tyr139 strengthens binding of the compound which has a K*i* value of 44.8 μM.

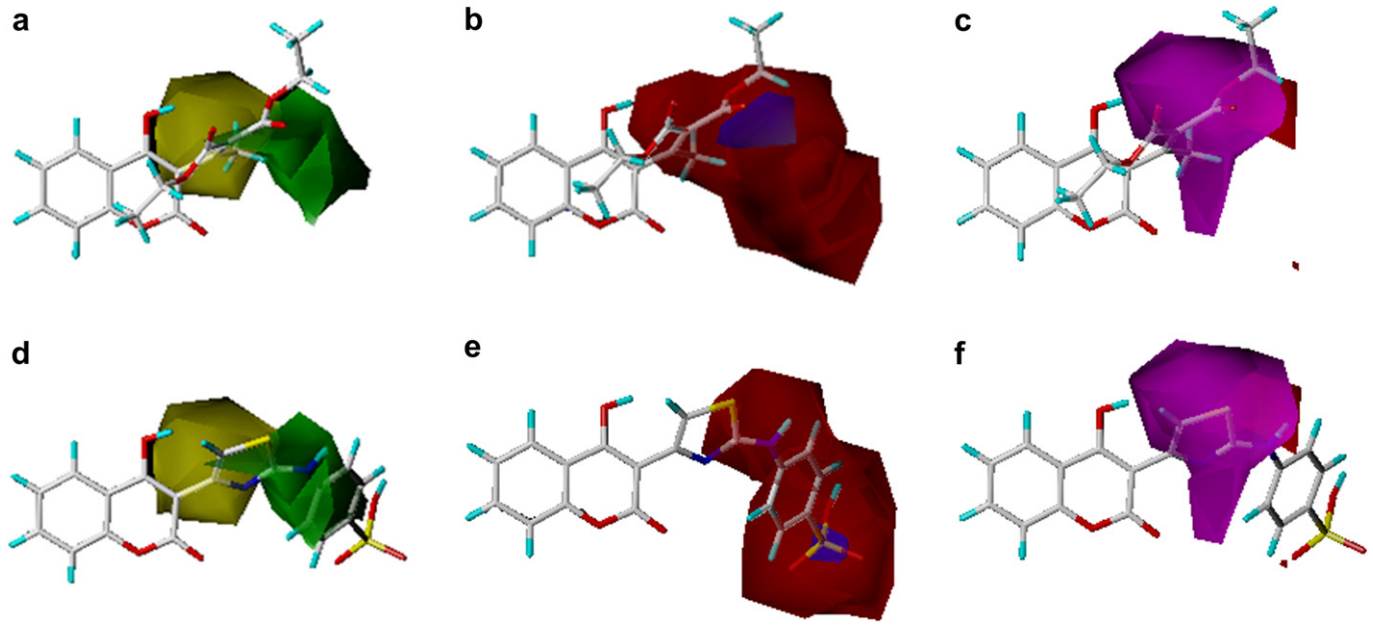

Fig. 4. CoMSIA a) Steric, b) Electrostatic and c) Hydrogen bond acceptor contour maps of **2b**; d) Steric, e) Electrostatic and f) Hydrogen bond acceptor contour maps of **4c**.

According to the results of molecular docking, higher activity of **2b** in comparison with **4c** can be attributed to the formation of more hydrogen bonds between **2b** and the active site of VKORC1.

The inhibition constants of **5c** and **9c** are 74.2 and 79.6 μM, respectively.

The binding of the lowest energy rank conformation of warfarin to VKORC1 occurs by formation of hydrogen bonds between the lactone carbonyl and the peptide bond of Tyr139 and Ala140, as well as between carbonyl group of phenylpentan-2-one residue and the peptide bond between Thr138 and Tyr139. Once again, orientation of the 4-OH group towards Cys135 is stabilized by Tyr139. The predicted K*i* of warfarin is 5.37 mM.

3.2.6. *Mechanistic studies of anticoagulant activity*

The exact mechanism of warfarin anticoagulant activity is a topic that is considered for decades. It is known that this drug acts as a competitive inhibitor of vitamin K-2,3-epoxide during its reduction catalyzed by VKORC1 [21]. Fasco *et al.* suggested that epoxide form undergoes the nucleophilic attack of negatively charged sulfur atom from the thiol group, side chain of the Cys catalytic site of VKORC1. This results with the formation of covalent bond between the enzyme and the substrate [21]. However, in work resulting in discovery of the VKORC1genes, Oldenburg *et al.* recently cited the Cys-SH form as the one involved in the epoxide reduction [3]. This mechanism was considered in the DFT studies of Deerfield *et al.*, as well, in which they suggested the formation of a covalent bond between the epoxide and the catalytic amino acid [8]. The reduction process is ended by the formation of a disulfide bond [4,21]. The SH form of catalytic amino acid was used in our mechanistic studies, too. The anticoagulant activity of warfarin is demonstrated by interaction of deprotonated open side chain coumarin form of the drug with amino acids of the catalytic site, leading to the interruption of vitamin K-2,3-epoxide reduction [3]. It was not specified whether the Cys132 or Cys135 amino acid is involved in interaction with anticoagulant or vitamin K-2,3-epoxide [3,21].

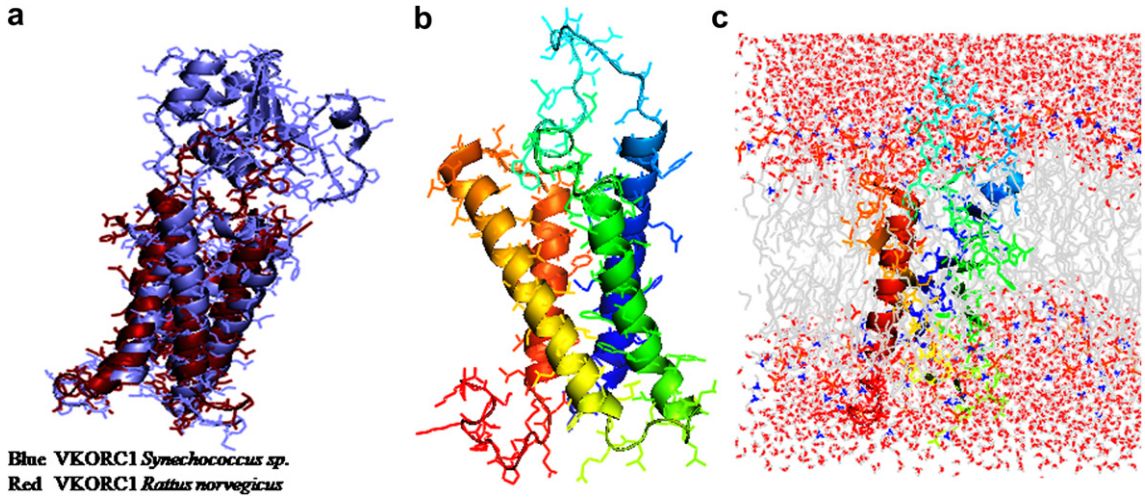

Fig. 5. a) A cartoon presentation of the alignment of the bacterial and rat VKORC1; b) α-Helixes and loops of homology-modeled VKORC1; c) Transmembrane rat VKORC1 system.

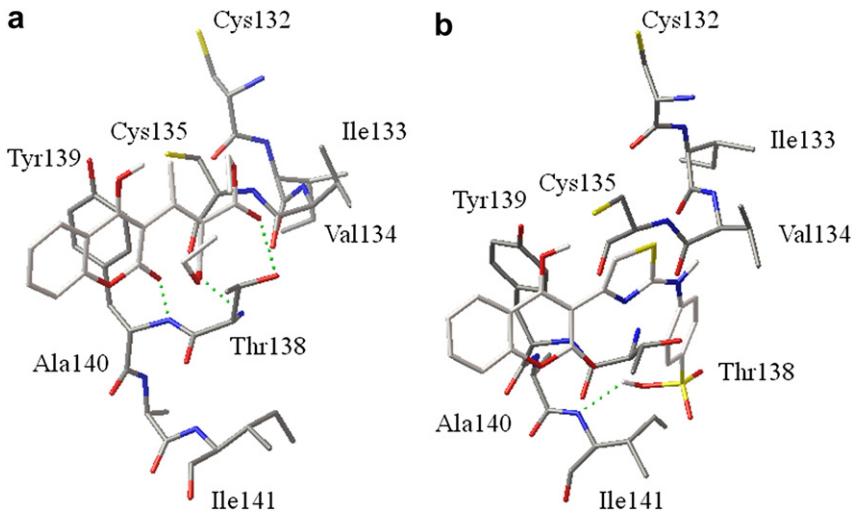

Fig. 6. Molecular docking conformations of a) **2b** and b) **4c**.

To become an anticoagulant agent, the coumarin molecule must be transformed into a structure similar to the quinone form of vitamin K epoxide. As an anticoagulant drug, warfarin exhibits chameleon-like isomerism, where the environment-dependent composition of the ensemble of structures greatly influences its bioavailability. It has been demonstrated by NMR-spectroscopic studies that warfarin exists in a state of dynamic equilibrium of seven different isomeric forms, with a distribution dependent on environmental factors, *e.g.* solvent polarity and pH [5]. As warfarin is transported to VKORC1 by binding to serum albumin in the open

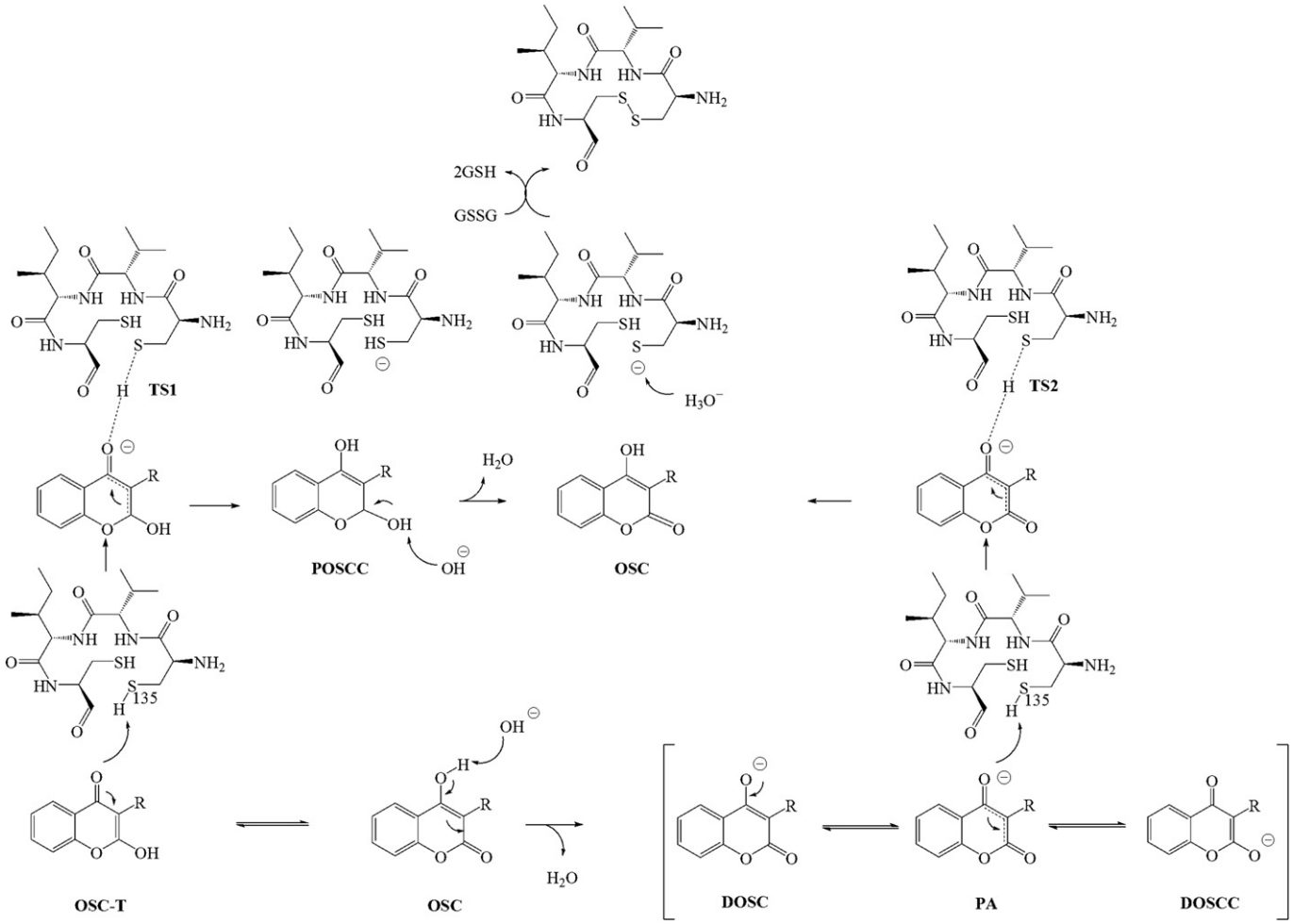

Scheme 3. The proposed mechanism of the coumarin antagonist activity.

side chain form, it is believed that its deprotonated form binds to the active site of VKORC1. Similarity between the structures of warfarin and vitamin K quinone form can be exhibited by even three major deprotonated open side chain forms of the drug [5]. All of these forms are considered in our vision of the mechanism regarding the anticoagulation activity of our compounds and warfarin. The problem in understanding the anticoagulant activity of warfarin starts with its inability to form the 4-hydroxycoumarin-2,3-epoxide and therefore a covalent bond with the catalytic amino acid. As a consequence, the warfarin antagonist form interacts with the active site of VKORC1 in other ways that are still debatable. There are no reported DFT studies that examine the role of warfarin or any coumarin compound in the neither inhibition mechanism nor coumarin interaction with the catalytic site of VKORC1.

In these DFT mechanistic studies describing anticoagulant activity of the tested compounds, we present possible ways of formation of the open side chain forms that may participate in inhibition of vitamin K-2,3-epoxide reduction during the coagulation cycle. In our opinion, the anticoagulant activity of evaluated compounds begins with binding of coumarin open side chain (**OSC**) form, *i.e.* the 4-OH coumarin form, to VKORC1 (Scheme 3) [6]. Several mechanistic pathways of **OSC** interaction with VKORC1 are proposed in a way that corresponds to warfarin behavior in an aqueous solution. The SH group of the catalytic amino acid Cys135, identified in the molecular docking studies, remains unchanged in the first step.

After formation of the coumarin-VKORC1 complex, the first reaction pathway possibly involves transformation of the **OSC** form to its isomeric open side chain tautomer (Scheme 3, **OSC-T**). Another transformation of **OSC** may occur after interaction of the coumarin inhibitor with the hydroxyl anion, a common species in cytoplasm, and formation of the deprotonated open side chain form (Scheme 3, **DOSC**). When **DOSC** form is formed, it is stabilized by intarmolecular delocalization leading to formation of a phenolic anion (Scheme 3, **PA**), a form that is similar to the quinone form of vitamin K-2,3-epoxide. The transformation of **PA** can further proceed to formation of the deprotonated open side chain chromone form (Scheme 3, **DOSCC**).

Thus, all of the structures, **OSC**, **OSC-T**, **DOSC**, and **DOSCC** are found in the warfarin aqueous solution and are structurally similar to the vitamin K quinone form, in conformity with Oldenburg's and Deerfield's consideration of the mechanism [3].

Selected coumarin derivatives are oriented towards the Cys135 in the active site of VKORC1 (Fig. 6., Scheme 3). The SH hydrogen atom of Cys135 can therefore be attacked by the 4-hydroxy group of **OSC-T**, **PA**, or even **DOSCC** (Scheme 3). During this step, the amino acid anion is formed, while coumarin regains the neutral **OSC** form. The final step of the mechanism is the spontaneous reformation of the SH bond of Cys135 by interaction with cellular protonium ion which is present to establish acid–base equilibrium. The process correlates with the Oldenburg's assertion that Cys-SH continues the mechanistic pathway until an S–S bond is formed. As the reaction itself occurs in the endoplasmic reticulum, the SH(Cys132) SH(Cys135) form is reduced by GSSG, but recent studies showed that even the negative form of SH(Cys135) can enter the reduction process [22].

The performed DFT studies revealed the reaction pathways by which coumarin antagonist forms arise and interact with the active site. Geometries of the **OSC** forms of **2b**, **4c**, **5c**, **9c**, and warfarin, were extracted from the complexes obtained by molecular docking and optimized in water as solvent. The energies of the optimized conformations were: 203.36, 207.98, 214.56, 208.89 and 197.64 kJ/mol for **2b** (Fig. 7., **OSC**), **4c** (Fig. 8., **OSC**), **5c**, **9c** and warfarin, respectively.

The proposed anticoagulant mechanism was computationally investigated step by step. In the mechanistic research, we were looking for the transition states that mediate all steps in the mechanism. Instead, it was found that transition states mediate only transfers of the SH hydrogen atom of Cys135 towards the **OSC-T** and **PA** forms of **2b**, **4c**, **5c**, **9c**, and warfarin (Figs. 7 and 8).

The energy profiles of the reaction between the tautomeric coumarin forms and Cys135 were investigated first. The energy value of the optimized **OSC-T-2b** form (203.42 kJ/mol) was comparable with the energy of **OSC-2b**. The slight difference in energy of the two forms suggested that tautomerisation occurs spontaneously

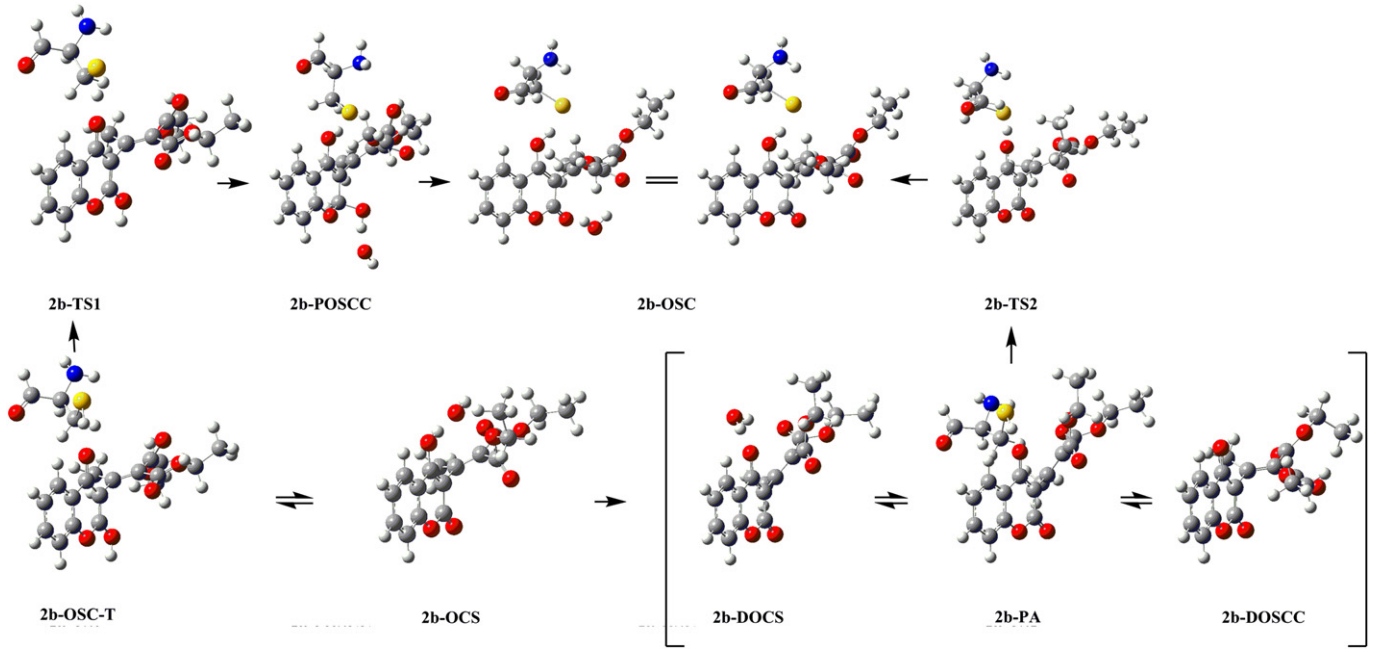

Fig. 7. DFT mechanistic study of anticoagulant activity of **2b**.

(Fig. 7.). Interaction between **OSC-2b** and Cys135 is mediated over the transition state **TS1**, formed after the amino acid SH proton has been attacked by the quinone-shaped 4-OH group. The starting geometries for transition state optimization were set with respect to distances between the SH and 4-OH groups that were revealed during the molecular docking. The activation energy for reformation of **OSC-2b** form was 4.97 kJ/mol. In the **TS1** arrangement, the lengths of Cys135····H and H····**2b** were 1.4794 and 1.4122 Å, respectively. The proposed mechanistic pathway also predicts the formation of unstable protonated open side chain chromone form (**POSCC-2b**), in which oxygen atoms of both lactone carbonyl and 4-OH group are substituted with a hydrogen atom. The equilibrium energy of **POSCC-2b** was 8.27 kJ/mol higher than the energy of **OSC-2b**. The energy difference is therefore used for the conversion of **POSCC-2b** to **OSC-2b**. It follows that the hydrogen atom of the newly formed lactone hydroxyl group spontaneously underlies attack of the cellular hydroxyl group, which results in the reformation of **OSC-2b**. The stabilization energy of the reaction was 196.58 kJ/mol.

Our attempts to optimize the interaction between the **OSC** form of **2b** and the hydroxide anion in the second proposed reaction pathway resulted in the spontaneous transfer (*i.e.* without any activation barrier) of a coumarin proton from the 4-OH group to the OH^- anion (Fig. 7.). This rearrangement includes creation of the **DOSC-2b** form and intarmolecular anion delocalization (**PA-2b**), with a system stabilization value of 194.19 kJ/mol. The lower value of equilibrium energy of **PA-2b** in comparison with **OSC-T-2b** suggested that the whole anticoagulant reaction is probably directed towards emergence of the **PA** rather than the **OSC-T** form. The reaction is further guided towards the formation of a negatively charged Cys135 sulfur atom. This process occurs after the abstraction of amino acid hydrogen atom by **PA** and restoration of the native coumarin form (**OSC**) *via* transition state **TS2**. Here again, the starting geometries for transition state optimization were set with respect to distances between the SH and 4-OH groups revealed after molecular docking. The activation energy for reformation of the **OSC-2b** was 4.91 kJ/mol. The lower activation barrier energy for the reaction between **PA** and Cys135, compared to **OSC-T**, is in agreement with the opinion that the deprotonated form of coumarin participates in the mechanism. In the **TS2** arrangement, the lengths of Cys135····H and H····**2b** were 1.4818 and 1.4126 Å, respectively.

Formation of the third deprotonated form, **DOSCC**, was proven to be energetically very unfavorable. The energy of the **DOSCC-2b** conformation was 26.42 kJ/mol higher than the energy of **OCS-2b**. As a consequence, all attempts to find the transition state between the **DOSCC** and Cys135 resulted in the reverse intramolecular stabilization of **DOSCC** to reformation of **PA**. The process is caused by the inability of the 4-OH group oxygen to accept a hydrogen atom due to electron deficiency of the oxygen itself.

Finally, we assumed that the negatively charged Cys135 sulfur atom is neutralized by the GSSH/2GSH system.

The mechanism of the anticoagulant activity of **4c**, **5c**, **9c**, and warfarin was considered in the same manner as for **2b**, according to energy profiles of reactions occurring *via* the proposed mechanisms. Thus, the activation barriers for the **TS1** and **TS2** arrangements were 8.86 and 8.02, 11.26 and 10.14, 11.36 and 10.88 kJ/mol and 17.24 and 16.35 kJ/mol, for **4c** (Fig. 8.), **5c**, **9c**, and warfarin, respectively.

The low value of the activation energy (*Ea*) of **TS2-2b** correlates perfectly with the highest activity *in vivo*. The rest of the calculated *Ea* values correlate nicely with the observed activity.

3.3. Design of novel coumarin anticoagulants and prediction of the activity

The manner in which prop-1-en-carbonyl/carboxyl and substituted *N*-thiazole moieties of the tested compounds contribute to anticoagulant activity is described above. On the basis of the material presented, we designed 16 novel improved coumarin structures (Scheme 4). Using obtained 3D-QSAR models, we calculated their pIC_{50} values for potential determination of anticoagulant activity *in vivo* (Table 3). The goal of the design was to successfully implement favorable functional groups, *i.e.* carboxyethyl, *p*-SO_3H, *m*-CH_3, and *m*-NO_2, on various coumarin structures. Pharmacophores were added to the modified warfarin core (**1d**, **7d**, **8d**, **13d**, **14d**, **15d**, and **16d**), 3-amino-4-hydroxycoumarin core (**5d** and **6d**), pyrano[3,2-c]chromene-2,5-dione core (**9d**, **10d**, **11d**), pyrano[3,2-c]chromen-5(4H)-one core (**12d**) and 4-hydroxycoumarin core

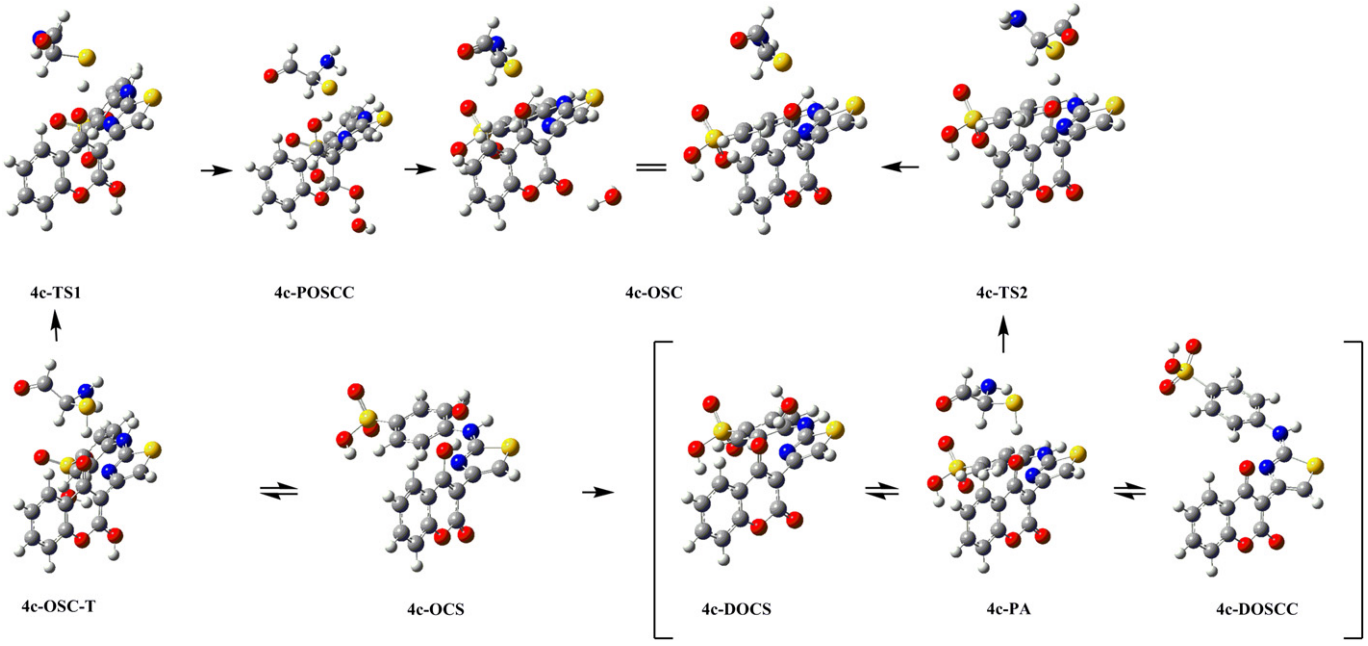

Fig. 8. DFT mechanistic study of anticoagulant activity of **4c**.

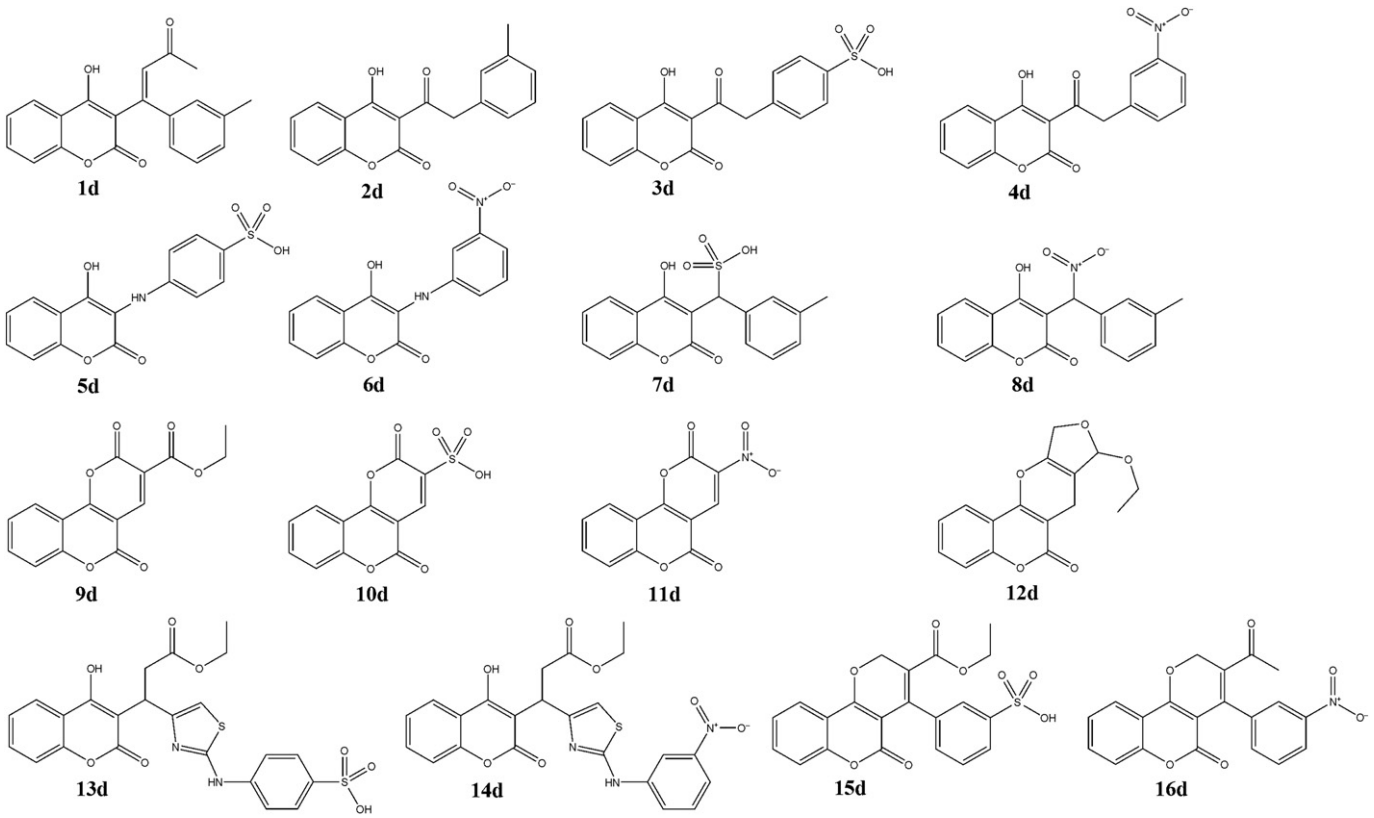

Scheme 4. Structures of newly designed coumarin anticoagulants.

(**2d**, **3d**, and **4d**). The novel structures were subjected to the same molecular modeling and 3D-QSAR methods applied for the tested compounds.

Use of 3D-QSAR methodology showed five of the designed compounds, **9d**, **7d**, **10d**, **15d** and **16d**, to be the most promising candidates (Table 3) for future synthesis and *in vivo* administration. The design was mainly oriented towards the introduction of groups like *p*-SO_3H, *m*-CH_3 and *m*-NO_2, which were concluded to be generally less toxic than the carboxyethyl one.

4. Conclusions

In evaluation of the *in vivo* anticoagulant activity of compounds **1**–**10c**, four of them (**2b**, **4c**, **5c** and **9c**) presented great potential. The most active compound was **2b** with a measured prothrombin time of 30 s. Evaluated compounds were confirmed as non-toxic agents by the appropriate biochemical analyses. Compounds were metabolized in the form of 7-hydroxycoumarin-glucuronides. The given activity was monitored on the level of molecular target, viz., homology-modeled rat VKORC1. 3D-QSAR and molecular docking studies revealed 4-OH group and C-3 diethylmalonate and thiazole-*N*-Ph-SO_3H scaffolds as pharmacophores that are mandatory for the activity. Also, DFT studies disclosed crucial interactions between the 4-O^- coumarin phenolic anion with Cys135, the catalytic center of VKORC1, during the prolongation of coagulation. The results of computational studies were further used for the design of novel compounds.

5. Experimental protocols

5.1. In vitro sample preparation

A frozen sample of human plasma, blood type A^+, was taken from Laboratory for Hematology, Clinical Hospital Center, Kragujevac, Serbia. All the coumarin samples were prepared according to Patent Application [23] for stable warfarin sodium liquid solutions (2 mL 96% EtOH, 1 mL 0.9% NaCl, 6 mL 20% glycerol and 1 mL of phosphate buffer, pH = 7), making 1 mg/mL solution.

5.2. Experimental conditions in vivo

5.2.1. Animals and in vivo sample preparation

Experiments were performed on 2.5 month-old adult albino Wistar rats, weighting 220–250 g, kept at 12 h dark/light intervals, 22 ± 2 °C and 50% relative humidity. The animals were fed with commercial rat food that was available *ad libitum*. All the animal procedures were approved by the Committee for Ethical Animal Care and Use of the Institute for Biological Research, Belgrade, which acts in accordance to the Guide for the Care and Use of Laboratory Animals, published by the US National Institute of Health (NIH Publication No. 85/23, revised in 1986). Two different coumarin concentrations, 0.1 and 0.5 mg/kg of body weight [24] were administrated to obtain a proper dose–response. The animals (three per each compound and control) were separated in three different groups. In the first two, animals were sacrificed 24 h after the administration of the 0.1 and 0.5 mg/kg coumarin solutions, respectively. In the third group, the animals were treated for five days, receiving one dose of 0.5 mg/kg per day. The animals were sacrificed on the sixth day. The ethanol solutions of tested compounds were administrated *intraperitoneal* (*i.p.*). The positive control was warfarin solution, while negative was 96% ethanol solution.

5.2.2. Coagulation and biochemical parameters

Plasma, for determination of prothrombin time, fibrin time and fibrinogen, and serum, for determination of biochemical parameters: bilirubin, AST, ALT, γ-GT, ALP, total amount of proteins,

albumins, globulins and Fe, were prepared by Quick method [25], immediately immersed in liquid nitrogen and stored at −80 °C. Coagulation experiments were performed on MYTHIC 22-Orphee hematology analyzer and THROMBOSTAT fibrintimer, while colorimetric measurements were recorded using a Perkin–Elmer Lambda 25 UV/Vis spectrophotometer.

The prothrombin time (PT) in both *in vitro* and *in vivo* experiments was measured by Quick method and the results are presented both in seconds and INR (Table 1). The IC_{50} values, *i.e.* the concentrations that increase prothrombin time for 50%, were calculated from linear dose-response curve [26] from the results obtained *in vivo*. Average PTs were taken for the compounds that have been administrated in 0.5 mg/kg concentration more than once. The IC_{50} values were used for the purpose of the *in vivo* 3D-QSAR studies. The IC_{50} values were converted into pIC_{50} by taking Log ($1/IC_{50}$). The coagulation time was determined by Howell method [27]. The activities of AST, ALT and γ-GT on 340 nm, and ALP on 405 nm, were determined by UV–Vis kinetic methods according to recommendations of the Expert Panel of the IFCC (International Federation of Clinical Chemistry) [28–30]. The colorimetric methods were used for determination of total bilirubin (Jendrassik–Grof 550 nm method) [31], serum iron (using Ferene as chromogen, on 595 nm) [32] proteins and fibrinogen concentration (biuret method on 540 nm) [33], albumin concentration (bromocresol green 628 nm method) [34] and the globulins as the difference in concentrations of total proteins and albumin.

5.2.3. Statistical evaluations

Statistical evaluation of the data was performed by 1-way analysis (ANOVA). Variance homogeneity and data distribution were determined with the Levene and Kolmogorov–Smirnov tests, respectively. Post-hoc comparison between control and treated groups was performed with the T3 Dunnett's test or with the Bonferroni test when the variance was not homogeneous. Statistical analysis was performed using the SPSS statistical software package, version 13.0 for Windows [35]. The results were considered to be statistically significant at $p < 0.05$.

5.2.4. Sample preparation for the determination of coumarin metabolites

Metabolic pathways of selected coumarin derivatives, **2b**, **4c**, **5c**, and **9c** were determined by new *i.p* administration, collection of the rat urine samples and following GC/MS analysis. New healthy animals were divided into the control ant test groups for the 72 h long application. Urine was collected on 24 h long intervals. Samples collected from the test group were used as a control and for assay validation. For validation, blank urine was spiked with appropriate amounts of selected compounds (0.5 μM) [36]. To 1 mL of spiked sample volume, 50 μL of formic acid (1 M) was added to give a final pH = 3.0–4.0. Collected urine samples were stored in deep freezing −80 °C conditions. Animals in the test group were treated for three days on 24 h long intervals by 1 mg/kg coumarin concentration. The second phase of coumarin rat metabolism normally occurs by glucuronidation of 7-hydroxycoumarin, which is the product of the first phase [19]. Therefore, after thawing, samples were hydrolyzed in order to detect the presence of 7-hydroxy forms of tested compounds. The 1 mL of urine samples was adjusted to about pH = 5.0 by addition of 100 μL acetate buffer (0.5 M) and incubated for 14 h at 37 °C in the presence of 50 μL of β-glucuronidase (9000 U/mL). Hydrolyzed samples were adjusted to pH = 3.0–4.0 by addition of 100 μL of formic acid (1 M).

5.2.4.1. Sample purification. Sample purification [36] was achieved using Sep Pak C_{18} light cartridges (130 mg, 1 mL) supplied by Waters (Eschborn, Germany). Samples were centrifuged at 17500 rpm for 10 min. After conditioning (1 mL of methanol) and equilibration (2 mL purified water), 1000 μL of the supernatant was passed through the cartridges with gentle positive-pressure at a flow rate of about 1.5 mL/min. After washing with 500 μL of acetonitrile/water 30/70% in 25 mM formic acid (pH = 3.0), the samples were eluted under basic conditions with 1000 μL of acetonitrile/water 40/60% in 25 mM ammonia (pH = 10.0). The eluates were subsequently centrifuged *in vacuo* for 30 min to a final volume of 500–600 μL. The volumes of 25 μL were injected into the GS/MS system.

5.2.4.2. GC/MS conditions. Metabolite screening was performed using a single-quadruple mass spectrometer (Hewlett Packard 6890N, Agilent Technologies, Santa Clara, CA, USA) with HP 5MS column, 30 m × 0.25 mm, i.d. film thickness 0.25 μm, operated by HP Enhanced ChemStation software. The analyses were performed in three consecutive steps. First step included scan mode fragmentation of ethanol solutions of **2b**, **4c**, **5c**, and **9c**. Spectrum of umbelliferone, a 7-hydoxycoumarin, was also recorded for the detection of M^+ ion. Second step included the scan and SIM (Selected ion monitoring) mode for the recognition of each applied compound in spiked urine samples. Final analysis included the scan and SIM mode for the recognition of each applied compound in hydrolyzed urine samples. The analytical conditions were set as follows: injector (splitless mode) and transfer line temperatures of 290 °C; oven temperature programmed at 200 °C with an increase of 15 °C/min to 290 °C (isothermal for 30 min); carrier gas helium at 1.3 ml min^{-1}; injection volume 3 μL; standard electronic impact MS source temperature 230 °C; MS quadruple temperature 150 °C; mass scan range 50–550 amu at 1800 eV; scan velocity 3.12 scans s^{-1}. SIM mode was chosen for the determination of the 7-hydroxy metabolites with a dwell time of 100 ms and same chromatographic conditions listed above. Following ions were monitored: *m*/*z* 91, 126, 147, 162 [20] and 362 for **2b**; *m*/*z* 91, 126, 147, 162 and 432 for **4c**; *m*/*z* 91, 126, 147, 162 and 366 for **5c**; *m*/*z* 91, 126, 147, 162 and 397 for **9c**.

5.3. Molecular modeling studies

5.3.1. Molecular optimization of coumarin compounds

The molecular optimizations were performed to determine the bioactive conformations of administrated coumarin compounds **1**–**10c**. The initial structures were built in Spartan 2008 [37] and imported in MacroModel 9.5 [38] *via* graphical interface Maestro 9.0. The conformations were obtained by using of the simulated annealing molecular dynamics procedure implemented in MacroModel as follows [39]. Each structure was energy minimized to a low gradient. The non-bonded cutoff distances for van der Waals interactions were set to 8 Å while distances for electrostatic ones were set to 20 Å. An initial random velocity to all atoms corresponding to 310 K was applied. Three subsequent molecular dynamics were then performed. The first was carried out for 10 ps with a 1.5 fs time-step at a constant temperature of 310 K for equilibration purposes. The next molecular dynamics was carried out for 20 ps, during which the system is coupled to a 150 K thermal bath with the time constant of 5 ps. The time constant represents approximately the half-life for equilibration with the bath; consequently the second molecular dynamics command caused the molecule to slowly cool to approximately 150 K. The third and last dynamics cooled the molecule to 50 K over 20 ps. A final energy minimization was then carried out for 250 iterations using conjugate gradient. The minimizations and molecular dynamics were in all cases performed by implicit salvation in simulated water

aqueous solution using GB/SA (Generalized Born solvent accessible surface area) keyword and the OPLS2005 force field.

5.3.2. Molecular alignment and CoMFA and CoMSIA modeling

CoMFA and CoMSIA models were obtained by using the Sybyl-X software of Tripos [40]. All of the molecules were aligned by an atom-by-atom least-square fit. The 2*H*-chromene structure was used as a template. For the purpose of the 3D-QSAR calculations, the compound's set was randomly divided into the training set (10 compounds) and the test-set (6 compounds). The subdivision was performed in such way that both sets represent equally well the chemical and biological properties of the whole data set. The CoMFA descriptor fields including the steric fields and the electrostatic fields were calculated at each lattice with grid spacing of 2 Å and extending to 4 Å units in all three dimensions within defined region. The van der Waals potentials and Coulombic terms, which represented steric and electrostatic fields, respectively, were calculated by using the standard Tripos force field. In CoMFA method, a sp^3 hybridized carbon atom with a charge of +1 was used as a probe atom, the energy values of the steric and electrostatic fields were truncated at 30 kcal/mol. The steric, electrostatic, hydrophobic, hydrogen bond donor and hydrogen bond acceptor CoMSIA potential fields were calculated at each lattice intersection of a regularly spaced grid of 2 Å and extending to 4 Å using a probe atom with radius 1.0 Å, +1.0 charge, and hydrophobic and hydrogen bond properties of +1. The attenuation factor was set to the default value of 0.3.

5.3.2.1. Partial least-squares (PLS) analysis. The partial least-squares (PLS) analysis was used to linearly correlate the CoMFA and CoMSIA fields to the pIC_{50} values. The cross-validation analysis was performed using the leave-one-out (LOO) method in which one molecule was removed from the data set and its activity was predicted using the model derived from the rest of the data set. The number of components in PLS models were optimized by using q^2 value, obtained from LOO cross-validation procedure. Column filtering was used at the default value of 2.0 kcal/mol in the cross-validation part. The final models were developed with ONC by using non-cross-validated analysis equal yielded the highest correlation coefficient (r^2).

5.4. Homology modeling of rat VKORC1

The *Rattus norvegicus* VKORC1 sequence was retrieved from publicly available sequence database Swiss-Prot/Uniprot (UniProt ID: Q6TEK4) [41]. On the base of the sequence search against the PDB, by using PSIBLAST, the crystallographic structure of *Synechococcus* sp. bacterial vitamin K epoxide reductase, at the resolution of 3.60 Å (PDB ID: 3KP9 chain A) [42], was identified as only and the best structural template (24.37% sequence identity) for the purpose of modeling the corresponding catalytic domain (Cys132-Cys135) of rat VKORC1. The alignment of the template and target sequences was carried out with CLUSTALW version 1.83 [43]. Swiss-Model [44], an automated comparative approach, was employed for the prediction of 3D rat VKORC1 structure, using alignment mode. The homology model quality was assessed by using PROCHECK [45] G-factor, with value of above −0.5.

5.4.1. Molecular dynamics of VKORC1

To perform a proper optimization of the newly generated transmembrane VKORC1 homology model, a membrane-aqueous system was built around the VKORC1 by using of phospholipide 1,2-dimiristoyl–SN–3-phosphorylcholine (DMPC) model (Fig. 5(**c**)). The entire protein-membrane-aqueous system was relaxed by conducted molecular dynamics simulation [46]. In the setup of the membrane system, pre-equilibrated conformers for each DMPC molecule were previously generated from the Monte Carlo simulations. This molecule set was developed at 340 K, above the gel-liquid-crystal phase transition temperature. After the formation of DMPC, system was annealed to 310 K. The membrane-protein system was built in Vega ZZ. In all, the complete membrane-aqueous system consisted of 161 amino acid residues, 128 DMPC molecules, 11 chlorine counter ions and 3655 water molecules. Molecular dynamics simulations were performed with NAMD [47] program, implemented in Vega ZZ [48] using the CHARMM22 PROT force field, after adding Gasteiger charges. Hydrogen atoms were added using the *psfgen* package. The starting system was relaxed by performing 10 000 steps of conjugate gradients energy minimization to remove unfavorable contacts, followed by 10 000 steps of MD at 310 K (equilibration phase). NAMD was used to perform 720 ps of MD simulation (with complete long-range electrostatic interactions) and with a time-step of 2 fs. The temperature was controlled *via* Langevin dynamics with a dumping factor of 5 ps^{-1}. Snapshot structures were extracted for every 1 ps, resulting 720 structures from each trajectory. Analysis of the trajectories was performed using Vega ZZ software package. All the calculations were performed at the dielectric constant value of $\varepsilon = 80.4$, in water as solvent. Thermodynamic properties, such as temperature and energy, were monitored during MD simulations to check their convergence to stable values. The average structure after equilibration was calculated and submitted to energy minimization performing 100 000 steps of conjugate gradients.

5.4.2. Molecular docking and energy minimization of ligand–enzyme complexes

The structure of newly generated rat VKORC1 protein was used in docking experiments. The structure was further manipulated by removing nonpolar hydrogen atoms, while Gasteiger charges and solvent parameters were added. All of the tested compounds were used as the ligands for docking. The rigid root and rotable bonds were defined using AutoDockTools. The docking was performed with AutoDock 4.2 [49]. The dimensions of the grids were thus 18 Å × 24 Å × 32 Å, with a spacing of 0.375 Å between the grid points and center grid box coordinates $x = 26.863$, $y = 68.637$, $z = 13.538$, referring to the enzyme active site: Thr138, Tyr139 and Ala140. The Lamarckian Genetic Algorithm was used to generate orientations or conformations of the ligand within the binding site. The global optimization started with a population of 200 randomly positioned individuals, a maximum of 1.0×10^6 energy evaluations and a maximum of 27 000 generations. A total of 100 runs were performed with RMS Cluster Tolerance of 0.5 Å.

Finally, a molecular mechanics approach was applied to refine the Autodock output. The computational protocol consisted the application of 10 000 steps of the steepest descent algorithm until the derivative convergence was 0.01 kcal/Å mol. AMBER force field with the continuum GB/SA salvation model (water as solvent) implemented in MacroModel was used during minimization. Moreover, because of the large number of atoms in the model, some additional constraints had to be imposed to correctly optimize the complexes obtained by the docking. A subset, comprising only the inhibitors and shells of residues possessing at least atom at a distance of 5 Å from any of the inhibitor atoms, was created and subjected to energy minimization. The inhibitors and all the amino acids side chains of the shell were unconstrained during energy minimization to allow the reorientation and proper hydrogen-bonding geometries and van der Walls contacts. All the atoms not included in the above-defined subset were fixed, but their nonbond interactions with all of the relaxing atoms have been calculated.

5.5. Coumarin VKORC1 inhibition reaction DFT mechanistic studies

We proposed the simple pseudo-enzymatic mechanism for our derivatives coagulation inhibition that was also applied for warfarin (Scheme 3, Fig. 7 and 8.). The mechanism is based on the recent views of Oldenburg *et al.* [3] and Deerfield *et al.* [8] on the roles of vitamin K and warfarin in the coagulation cycle.

Mechanistic calculations on the selected structures were performed with Gaussian 03 software [50]. Starting geometries of most active compounds *in vivo*, **2b**, **4c**, **5c**, and **9c**, were optimized using DFT B3LYP functional and 6-311G(d,p) level of theory. The geometrical parameters of all stationary points were optimized in water ($\varepsilon = 78.36$) using the CPCM solvation model. All calculated structures were confirmed to be local minima (all positive eigenvalues) for ground state structures. The transition state geometries (TS) were built by Gaussview 3.07 and calculated with DFT B3LYP functional and 6-311G++(d,p) level of theory, in water ($\varepsilon = 78.36$) by using the CPCM solvation model. All calculated transition state structures were confirmed to be first-order saddle points (one negative eigenvalue), by frequency calculations. The intrinsic reaction coordinates (IRCs), from the transition states down to the two lower energy structures, were traced using the IRC routine in Gaussian in order to verify that each saddle point is linked with two putative minima. The results of the IRC calculations for one crucial transition state, TS, are presented in Fig. 7. Evolution of relevant bonds along the reaction pathway was estimated using the natural bond orbital analysis.

Acknowledgments

This work was financed by Government of the Republic of Serbia, Ministry of Education and Science, Grants No. III 43004, III 41010 and OI 173020. The authors would like to thank Professor Dr Svetlana Marković, Department of Chemistry, Faculty of Science, Kragujevac, Serbia, for useful suggestions on Gaussian computational modeling. The authors have declared no conflict of interest.

References

[1] P.M. Ridker, S.Z. Goldhaber, E. Danielson, Y. Rosenberg, C.S. Eby, S.R. Deitcher, M. Cushman, S. Moli, C.M. Kessler, C.G. Eliot, R. Paulson, T. Wong, K.A. Bauer, B.A. Shwartz, J.P. Miletich, H. Baounameaux, R.J. Glyn, N. Engl. J. Med. 348 (2003) 1425–1434.
[2] J. Hirch, V. Fuster, J. Aussel, J.L. Halpelin, J. Am. Coll. Cardion. 41 (2003) 1633–1652.
[3] J. Oledbnburg, M. Watzka, S. Rost, C.R. Muller, J. Thromb. Haemost. 5 (s1) (2007) 1–6.
[4] I. Petitpas, A.A. Bhattacharya, S. Twine, M. Twine, M. East, S. Curry, J. Biol. Chem. 276 (2001) 22804–22809.
[5] B.C.G. Karlsson, A.M. Rosengren, P.O. Andersson, I.A. Nicholls, J. Phys. Chem. 111 (2007) 10520–10528.
[6] H. Henschel, B.C.G. Karlsson, A.M. Rosengren, I.A. Nicholls, J. Mol. Struc:-THEOCHEM 958 (2010) 7–9.
[7] D. Lafitte, V. Lamour, P. Tsvetkov, A.A. Markov, M. Deprez, P. Klich, D. Moras, C. Briand, R. Gilli, Biochemistry 41 (2002) 7217–7223.
[8] D.E. Deerfield II, C.H. Davis, T. Wymore, D.W. Stafford, L.G. Pedesen, Int. J. Quantum Chem. 106 (2006) 2944–2952.
[9] M. Grauber, Bioorg. Med. Chem. 15 (2007) 2414–2420.
[10] M. Mladenović, N. Vuković, N. Nićiforović, S. Sukdolak, S. Solujić, Molecules 14 (2009) 1495–1512.
[11] N. Vuković, S. Sukdolak, S. Solujić, T. Milosević, Arch. Pharm. 341 (2008) 491–496.
[12] N.P. Singh, Mutat. Res. 455 (2000) 111–127.
[13] B.C. Tennant, Clinical biochemistry of laboratory animals, in: W.F. Loeb, F.W. Quimby (Eds.), Assessment of Hepatic Function, Taylor and Francis, London, 1999, pp. 501–517.
[14] M. Shah, P. Patel, M. Phadke, S. Menon, F. Mary, T. Saner, Indian Drugs 39 (2002) 333–337.
[15] S. Manokaran, A. Jaswanth, S. Sengottuvelu, J. Nandhakumar, R. Duraisamy, D. Karthikeyan, R. Mallegaswari, Res. J. Pharm. Tech. 1 (2008) 398–401.
[16] Y.K. Gupta, M. Sharma, G. Chaudhary, Methods Find. Exp. Clin. Pharmacol. 24 (2002) 451–497.
[17] Y.K. Gupta, M. Sharma, G. Chaudhary, C.K. Katiyar, Phytother. Res. 18 (2004) 362–364.
[18] R.K. Murray, D.K. Granner, P.A. Mayes, V.W. Rodwell, Enzymes: mechanism of action, in: V.W. Rodwell, P.J. Kennelly (Eds.), Harper's Illustrated Biochemistry, twenty-sixth ed. The McGraw-Hill Companies/Lange Medical Books, New York, 2003, pp. 49–60.
[19] O. Pelkonen, H. Raunio, A. Rautio, J. Maenpaa, M.A. Lang, J. Irch. Coll. Phys. Surg. 22 (1993) 24–28.
[20] N.S. Vul'fson, V.I. Zaretskii, V.G. Zaikin, Russ. Chem. Bull. 12 (1963) 2046–2049.
[21] M.J. Fasco, L.M. Principe, J. Biol. Chem. 10 (1982) 4894–4901.
[22] C.S. Sevier, C.A. Kaiser, Nat. Rev. Mol. Cell Biol. 3 (2002) 836–847.
[23] M.E. Anderson, D. Delmarre, D. Gao, M.A. El-khateeb, C.S. Certeno, S.H. Pathak, PCT/US2006/023438. 2006.
[24] M. Kataranovski, J. Živanović, J. Vranković, I. Mirkov, D. Kataranovski, Arch. Biol. Sci. 59 (2007) 53–54.
[25] A.J. Quick, M. Stanley-Brown, F.W. Bancroft, Am. J. Med. Sci. 190 (1935) 501.
[26] M.S. Bhatia, K.B. Ingale, P.B. Choudhari, N.M. Bhatia, R.L. Sawant, Bioorg. Med. Chem. 17 (2009) 1654–1662.
[27] W.H. Howell, Physiol. Rev. 15 (1935) 435–470.
[28] H.U. Bergmeyer, G.N. Bowers, M. Hørder, D.W. Moss, Clin. Chim. Acta 70 (1976) 19–42.
[29] H.U. Bergmeyer, Clin. Chim. Acta 105 (1980) 147–172.
[30] M.I. Walters, H.W. Gerarde, Microchem. J. 15 (1970) 231–243.
[31] L. Jendrassik, P. Gróf, Biochem. Z. 297 (1938) 82–89.
[32] F. Ceriotti, G. Ceriotti, Clin. Chem. 26 (1980) 327–331.
[33] A.G. Gornall, C.J. Bardawill, M.M. David, J. Biol. Chem. 177 (1949) 751–766.
[34] P.H. Lolekha, W. Charoenpol, Clin. Chem. 20 (1974) 617–619.
[35] S.J. Coakes, L. Steed, P. Dzidic, SPSS Version 13.0 for Windows: Analysis Without Anguish, John Wiley & Sons Australia, Milton, Qld., 2006.
[36] M. Ufer, B. Kammerer, J. Kirchheiner, A. Rane, J. Swensson, J. Chromat. B 809 (2004) 217–226.
[37] Software Spartan 2006 for Windows, Wavefunction, Inc., USA, 2006.
[38] F. Mohamadi, N. Richards, W. Guida, R. Liskamp, M. Lipton, C. Caulfield, G. Chang, T. Hendrikson, W. Still, J. Comput. Chem. 11 (1990) 440–467.
[39] R. Ragno, S. Simeoni, D. Rotili, A. Caroli, G. Botta, G. Brosch, S. Massa, A. Mai, Eur. J. Med. Chem. 43 (2008) 621–632.
[40] Sybyl Version X1.1, St. Tripos Associates Inc, Louis (MO), 2010.
[41] B. Boeckmann, A. Bairoch, R. Apweiler, M.C. Blatter, A. Estreicher, E. Gasteiger, M.J. Martin, K. Michoud, C. O'Donovan, I. Phan, S. Pilbout, M. Schneider, Nucleic Acids Res. 31 (2003) 365–370.
[42] W. Li, S. Schulman, R.J. Dutton, D. Boyd, J. Beckwith, T.A. Rapoport, Nature 463 (2010) 507–512.
[43] J.D. Thompson, D.G. Higgins, T.J. Gibson, Nucleic Acids Res. 22 (1994) 4673–4680.
[44] J. Kopp, T. Schwede, Nucleic Acids Res. 32 (2004) 230–234.
[45] R.A. Laskowski, M.W. MacArthur, D.S. Moss, J.M. Thornton, J. Appl. Cryst. 26 (1993) 283–291.
[46] Y. Zhang, Y.Y. Sham, R. Rajamani, J. Gao, P. Portoghese, ChemBioChem. 6 (2005) 853–859.
[47] J.C. Phillips, R. Braun, W. Wang, J. Gumbart, E. Tajkhorshid, E. Villa, C. Chipot, R.D. Skeel, L. Kale, K. Schulten, J. Comput. Chem. 26 (2005) 1781–1802.
[48] A. Pedretti, A. Villa, G. Vistoli, J. Mol. Graph. Model. 21 (2002) 47–49.
[49] M.G. Morris, S.D. Goodsell, R. Huey, J.A. Olson, J. Comp. Aid. Mol. Des. 10 (1996) 293–304.
[50] M.J. Frisch, G.W. Trucks, H.B. Schlegel, G.E. Scuseria, M.A. Robb, J.R. Cheeseman, G. Scalmani, V. Barone, B. Mennucci, G.A. Petersson, H. Nakatsuji, M. Caricato, X. Li, H.P. Hratchian, A.F. Izmaylov, J. Bloino, G. Zheng, J.L. Sonnenberg, M. Hada, M. Ehara, K. Toyota, R. Fukuda, J. Hasegawa, M. Ishida, T. Nakajima, Y. Honda, O. Kitao, H. Nakai, T. Vreven, J.A. Montgomery, J.E. Peralta Jr., F. Ogliaro, M. Bearpark, J.J. Heyd, E. Brothers, K.N. Kudin, V.N. Staroverov, R. Kobayashi, J. Normand, K. Raghavachari, A. Rendell, J.C. Burant, S.S. Iyengar, J. Tomasi, M. Cossi, N. Rega, J.M. Millam, M. Klene, J.E. Knox, J.B. Cross, V. Bakken, C. Adamo, J. Jaramillo, R. Gomperts, R.E. Stratmann, O. Yazyev, A.J. Austin, R. Cammi, C. Pomelli, J.W. Ochterski, R.L. Martin, K. Morokuma, V.G. Zakrzewski, G.A. Voth, P. Salvador, J.J. Dannenberg, S. Dapprich, A.D. Daniels, Ö. Farkas, J.B. Foresman, J.V. Ortiz, J. Cioslowski, D.J. Fox, Gaussian 03 C02, Gaussian, Inc., Wallingford CT, 2004.